Effects of rising CO_2 on the harmful cyanobacterium Microcystis

Sandrini, G.

Publication date
2016
Document Version
Final published version

Chapter 3

Changes in gene expression, cell physiology and toxicity of the harmful cyanobacterium *Microcystis aeruginosa* at elevated CO_2

Changes in gene expression, cell physiology and toxicity of the harmful cyanobacterium *Microcystis aeruginosa* at elevated CO_2

Giovanni Sandrini[1], Serena Cunsolo[1], J. Merijn Schuurmans[1,2], Hans C. P. Matthijs[1], Jef Huisman[1]

[1]*Department of Aquatic Microbiology, Institute for Biodiversity and Ecosystem Dynamics, University of Amsterdam, Amsterdam, The Netherlands*
[2]*Department of Aquatic Ecology, Netherlands Institute of Ecology, Wageningen, The Netherlands*

Keywords: bicarbonate uptake; climate change; CO_2-concentrating mechanisms; harmful algal blooms; inorganic carbon uptake; microarrays; microcystins; phytoplankton

This chapter is published as:
Sandrini G, Cunsolo S, Schuurmans JM, Matthijs HCP, Huisman J. (2015). Changes in gene expression, cell physiology and toxicity of the harmful cyanobacterium *Microcystis aeruginosa* at elevated CO_2. *Frontiers in Microbiology* **6:** 401.

Abstract

Rising CO_2 concentrations may have large effects on aquatic microorganisms. In this study, we investigated how elevated pCO_2 affects the harmful freshwater cyanobacterium *Microcystis aeruginosa*. This species is capable of producing dense blooms and hepatotoxins called microcystins. Strain PCC 7806 was cultured in chemostats that were shifted from low to high pCO_2 conditions. This resulted in a transition from a C-limited to a light-limited steady state, with a ~2.7 fold increase of the cyanobacterial biomass and ~2.5 fold more microcystin per cell. Cells increased their chlorophyll *a* and phycocyanin content, and raised their PSI/PSII ratio at high pCO_2. Surprisingly, cells had a lower dry weight and contained less carbohydrates, which might be an adaptation to improve the buoyancy of *Microcystis* when light becomes more limiting at high pCO_2. Only 234 of the 4691 genes responded to elevated pCO_2. For instance, expression of the carboxysome, RuBisCO, photosystem and C metabolism genes did not change significantly, and only a few N assimilation genes were expressed differently. The lack of large-scale changes in the transcriptome could suit a buoyant species that lives in eutrophic lakes with strong CO_2 fluctuations very well. However, we found major responses in inorganic carbon uptake. At low pCO_2, cells were mainly dependent on bicarbonate uptake, whereas at high pCO_2 gene expression of the bicarbonate uptake systems was down-regulated and cells shifted to CO_2 and low-affinity bicarbonate uptake. These results show that the need for high-affinity bicarbonate uptake systems ceases at elevated CO_2. Moreover, the combination of an increased cyanobacterial abundance, improved buoyancy, and higher toxin content per cell indicates that rising atmospheric CO_2 levels may increase the problems associated with the harmful cyanobacterium *Microcystis* in eutrophic lakes.

Introduction

Cyanobacterial blooms are a well-known cause of nuisance in eutrophic lakes (Chorus and Bartram, 1999; Huisman *et al.*, 2005; Merel *et al.*, 2013). They may increase the turbidity of the water column, suppressing the growth of submerged water plants (Scheffer, 1998), and can produce considerable odor and taste problems (Watson *et al.*, 2008). Moreover, cyanobacteria can produce a variety of potent toxins, including microcystins and anatoxins, which cause liver, digestive and neurological disease in birds, mammals and humans (Jochimsen *et al.*, 1998; Carmichael, 2001; Codd *et al.*, 2005). This has led to the closure of lakes and reservoirs for recreational use, aquaculture, drinking water and irrigation water, often with considerable economic damage as a result (Verspagen *et al.*, 2006; Dodds *et al.*, 2008; Qin *et al.*, 2010).

Several studies warn of an intensification of cyanobacterial blooms in eutrophic waters, due to the combination of global warming (Jöhnk *et al.*, 2008; Paerl and Huisman,

2008; O'Neil *et al.*, 2012) and rising CO_2 concentrations in the atmosphere (Verschoor *et al.*, 2013; Verspagen *et al.*, 2014a, 2014b). The dissolved inorganic carbon (C_i) concentration in eutrophic lakes can vary strongly. Many lakes are supersaturated with dissolved CO_2 (CO_2(aq)) with concentrations that can go up to 10,000 ppm (Cole *et al.*, 1994; Sobek *et al.*, 2005; Lazzarino *et al.*, 2009), but lakes with high photosynthetic activities of dense cyanobacterial blooms have often undersaturating CO_2(aq) concentrations (Ibelings and Maberly, 1998; Balmer and Downing, 2011; Verspagen *et al.*, 2014b). Depletion of CO_2(aq) during cyanobacterial blooms is accompanied by a strong increase in pH (Talling, 1976; Jeppesen *et al.*, 1990; López-Archilla *et al.*, 2004). With increasing pH, the speciation of dissolved inorganic carbon shifts from CO_2(aq) towards bicarbonate (HCO_3-) and carbonate (CO_3^{2-}). Because phytoplankton species differ in their uptake rates of CO_2(aq) and bicarbonate (Rost *et al.*, 2003; Price *et al.*, 2008; Maberly *et al.*, 2009), these changes in carbon speciation may strongly affect competitive interactions between the species (Tortell *et al.*, 2002; Rost *et al.*, 2008; Verschoor *et al.*, 2013). In particular, cyanobacteria are believed to be very efficient competitors at low CO_2 conditions (Shapiro, 1997).

Many cyanobacteria have evolved a highly efficient CO_2-concentrating mechanism (CCM) to proliferate at low ambient CO_2(aq) levels and to overcome the low affinity of the primary CO_2 fixing enzyme, RuBisCO (Giordano *et al.*, 2005; Price *et al.*, 2008; Raven *et al.*, 2012). The CCM of cyanobacteria works quite differently from CCMs found in eukaryotic algae. In the latter, a pH gradient across the chloroplast thylakoid membrane in the light secures C_i accumulation in the cytosol (Moroney and Ynalvez, 2007). In cyanobacteria, the CCM is based on accumulation of bicarbonate in specialized compartments, called carboxysomes, that contain the RuBisCO enzyme. Conversion of bicarbonate inside the carboxysomes by carbonic anhydrases raises the local CO_2 concentration, near RuBisCO, which can then efficiently fix CO_2 (Price *et al.*, 2008). However, photorespiration and Mehler-like reactions have also been identified in cyanobacteria, signifying that cyanobacterial photosynthesis can still be limited by a low C_i availability despite their CCM (Helman *et al.*, 2005; Zhang *et al.*, 2009; Hackenberg *et al.*, 2012). Up to four flavodiiron proteins (Flv1-4) are involved in the low C_i adaptation process, acting as an electron sink at photosystem I (PSI, for Flv1,3) and photosystem II (PSII, for Flv2,4) (Zhang *et al.*, 2012; Allahverdiyeva *et al.*, 2011; Bersanini *et al.*, 2014).

The CCMs of fully sequenced cyanobacteria, like *Synechocystis* PCC 6803 and several *Synechococcus* strains, have been studied in detail (Omata *et al.*, 1999; Price *et al.*, 2004; Schwarz *et al.*, 2011). This has revealed that cyanobacteria have several different C_i uptake systems: three systems for bicarbonate uptake have been identified and two systems for CO_2 uptake (Price, 2011). BicA and SbtA are both sodium-dependent bicarbonate symporters. BicA

has a low affinity and high flux rate, whereas SbtA has a high affinity and low flux rate (Price *et al.*, 2004). The third bicarbonate uptake system, BCT1, has direct ATP-dependent functionality and consists of four subunits (CmpABCD). BCT1 has a relatively high affinity for bicarbonate and low flux rate, although its affinity is slightly lower than that of SbtA (Omata *et al.*, 1999, 2002; Price *et al.*, 2008). The two CO_2 uptake systems, NDH-I_3 and NDH-I_4, convert CO_2 that passively diffuses into the cell to bicarbonate, and consist of multiple subunits (Price, 2011). The two CO_2 uptake systems are likely NADPH-dependent (Price *et al.*, 2002). Functionally, NDH-I_3 has a high substrate affinity and low flux rate, whereas NDH-I_4 combines a lower substrate affinity with a higher flux rate (Maeda *et al.*, 2002; Price *et al.*, 2002).

From an environmental and ecological perspective, the harmful cyanobacterium *Microcystis aeruginosa* (hereafter called *Microcystis*) is of great interest. *Microcystis* is one of the more notorious cyanobacterial species, producing dense and often toxic blooms in eutrophic lakes all over the world (Chen *et al.*, 2003; Verspagen *et al.*, 2006; Michalak *et al.*, 2013). Now that full genome analysis has been completed for a range of different Microcystis strains (*e.g.*, Kaneko *et al.*, 2007; Frangeul *et al.*, 2008; Humbert *et al.*, 2013), knowledge on carbon acquisition is available, which enables detailed study of the response of *Microcystis* to rising CO_2 levels. Selection experiments have shown that rising CO_2 levels may shift the competitive balance between toxic and nontoxic *Microcystis* strains (Van de Waal *et al.*, 2011). Furthermore, the genetic diversity of the CCM in different *Microcystis* strains was recently elucidated (Sandrini *et al.*, 2014). This revealed that all investigated *Microcystis* strains contained genes encoding the two CO_2 uptake systems, the bicarbonate uptake system BCT1 and several carbonic anhydrases, but the strains differ in the presence of the bicarbonate uptake genes *bicA* and *sbtA*.

In this study, we investigate the response of the toxic *Microcystis* strain PCC 7806 to rising CO_2 levels, and how its gene expression and cell physiology, including the presence of its toxin microcystin, change at elevated pCO_2. For this purpose, *Microcystis* was cultivated in controlled laboratory chemostats that were shifted from low to high pCO_2 conditions. We provided the chemostats with a low CO_2 partial pressure (pCO_2) of 200 ppm to create C_i-limited conditions. After 36 days, we raised the pCO_2 level to 1450 ppm pCO_2, which is a representative level for many supersaturated lakes (Sobek *et al.*, 2005). Our results show that elevated CO_2 leads to a highly specific transcriptome response of *Microcystis*, and affects the C_i uptake, biomass, cellular composition and toxicity of *Microcystis* cells.

Results

Population dynamics and inorganic carbon chemistry

During the first phase of the experiment, we used a low pCO_2 concentration in the gas flow of 200 ppm to create C_i-limited conditions. In all four replicate chemostats, the cyanobacterial abundance gradually increased over time and approached a steady state after ~17 days (**Figure 3.1A**). Cell growth in the chemostats attenuated the light passing through, so that the light penetration I_{out} at this first steady state was reduced to ~6 µmol photons m^{-2} s^{-1} (**Figure 3.1A**). The CO_2(aq) concentration was depleted to the nano-molar range (**Figure 3.1B**). This was accompanied by a rise in pH to ~11, a strong decrease in bicarbonate concentration to ~60 µmol L^{-1} and a strong increase in carbonate concentration to ~300 µmol L^{-1} (**Figure 3.1B,C**). The total DIC concentration was not much affected during this first phase of the experiment (**Figure 3.1C**).

After 36 days, we raised the pCO_2 level in the gas flow to 1450 ppm pCO_2. The transition from 200 to 1450 ppm led to major changes in pH and inorganic carbon chemistry (**Figure 3.1B,C**; **Figure S3.1, Supplementary Information**). Within 24 h, the CO_2(aq) concentration increased over more than four orders of magnitude to ~30 µmol L^{-1}, while the pH dropped back from 11 to 8 and the bicarbonate concentration increased to ~2,000 µmol L^{-1} (**Figure S3.1, Supplementary Information**).

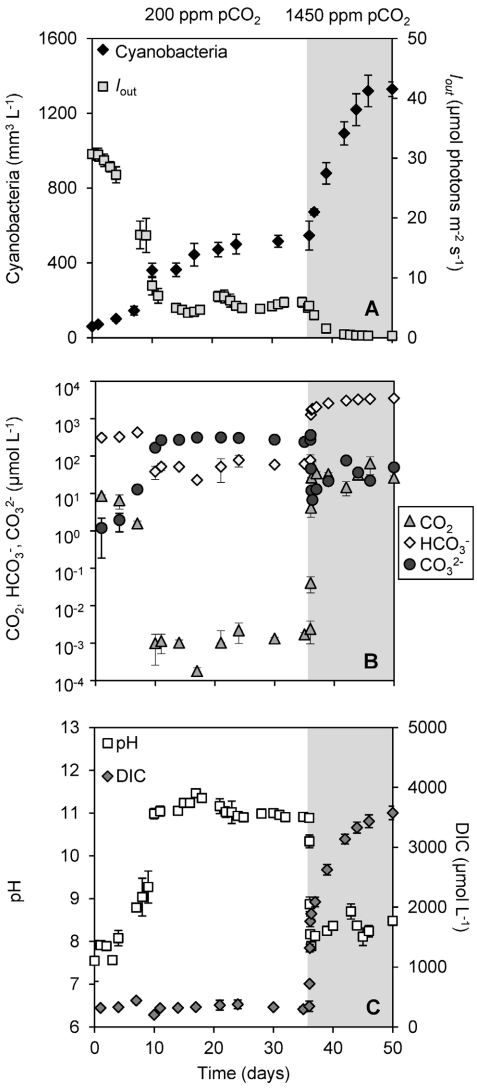

Figure 3.1. Changes in cyanobacterial abundance, light, dissolved inorganic carbon (DIC) and pH during a shift from low pCO_2 (200 ppm, *white area*) to high pCO_2 (1450 ppm, *shaded area*). (A) Cyanobacterial abundance (expressed as biovolume) and light intensity penetrating through the chemostat (I_{out}). **(B)** Dissolved CO_2 (CO_2), bicarbonate (HCO_3^-) and carbonate (CO_3^{2-}) concentrations (logarithmic scale). **(C)** Dissolved inorganic carbon (DIC) and pH. Error bars indicate standard deviations (n = 4).

The enhanced CO_2 availability alleviated the cyanobacteria from C_i limitation, thus enabling a strong increase in cyanobacterial abundance (**Figure 3.1A**). The resultant high biomass effectively absorbed all incident light, reducing light penetration through the chemostats to Iout < 0.1 µmol photons m^{-2} s^{-1} (**Figure 3.1A**). Nitrate uptake by the growing cyanobacterial population increased alkalinity (**Figure S3.2, Supplementary Information**), which initiated a progressive further increase of the DIC concentration (**Figure 3.1C**). After 46 days a new steady state was attained, with a ~2.7 fold higher cyanobacterial abundance than the previous steady state, a DIC concentration of ~3,500 µmol L^{-1} consisting largely of bicarbonate and CO_2, but low light conditions (**Figure 3.1A-C**).

Cell volume, cell weight and cellular composition

Although the cell volume of *Microcystis* was hardly affected by the elevated pCO_2, the average dry weight of the cells decreased by 50%, from 12 to 6 pg $cell^{-1}$ (**Figure 3.2A**). This was accompanied by a decrease of the C and N content of the cells at elevated pCO_2 (**Figure 3.2B**). Remarkably, the molar C/N ratio of the cells also slightly decreased at elevated pCO_2 (**Figure 3.2C**), despite the strong increase in C_i availability.

Major macromolecules (carbohydrates, proteins and lipids) and phosphate stored in the cells were quantified just before and 2 weeks after raising the pCO_2 level (**Figure 3.2D**). The carbohydrate content (expressed as % dry weight) decreased significantly (Student *t*-test: $t_6 = 4.6$, $p < 0.01$), whereas the protein content increased significantly at elevated pCO_2 (Student *t*-test: $t_6 = -6.8$, $p < 0.001$) (**Figure 3.2D**), which is consistent with the decrease of the cellular C/N ratio (**Figure 3.2C**). Lipids and phosphate contributed less to the total average cell weight than carbohydrates. Genes involved in carbohydrate storage and polyhydroxyalkanoate (PHA) storage showed no large changes in expression during the experiment, although minor upregulation of the *pha* genes was noticeable 8 h after the switch to high pCO_2 (**Table 3.1**).

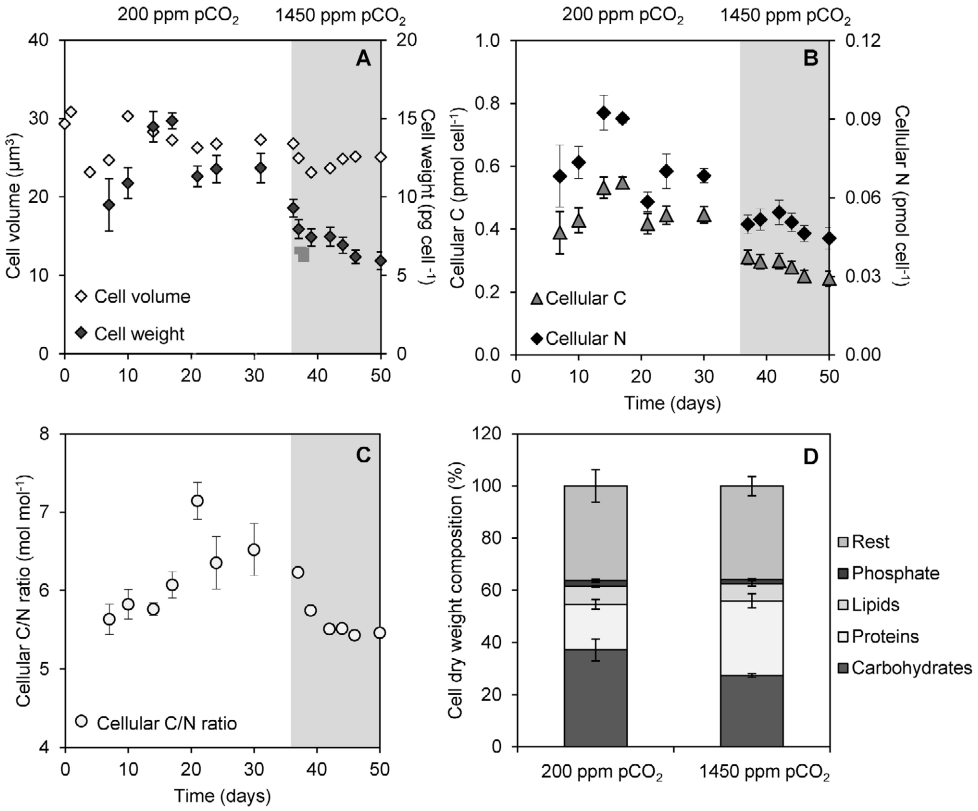

Figure 3.2. Changes in cell properties during a shift from low pCO_2 (200 ppm, *white area*) to high pCO_2 (1450 ppm, *shaded area*). (A) Average cell volume and cell weight. **(B)** Cellular elemental C and N content. **(C)** Molar C/N ratio of the cells. **(D)** Dry weight composition of cells from the steady states at 200 and 1450 ppm pCO_2. Error bars indicate standard deviations (n = 4).

Pigments and photosystems

Light absorption spectra normalized at 750 nm indicated that the cellular contents of the pigments chlorophyll *a*, phycocyanin and β-carotene increased at elevated pCO_2 (**Figure 3.3A**). The phycocyanin peak (at 626 nm) increased slightly more than the chlorophyll *a* peak (at 678 nm). The ratio of PSI to PSII changed, with less PSII and more PSI at elevated pCO_2 (**Figure 3.3B**). Yet, only a few genes involved in pigment synthesis and none of the photosystem genes changed expression significantly after exposure to high pCO_2 (**Table 3.1**).

Table 3.1. Genes responding to rising pCO_2 and involved in pigment synthesis, photosystems, C metabolism, C storage, N assimilation and stress response.

Gene or IPF number[a]	Gene function category[b]	Annotation[c]	Log2 values at different time points (h)[d]						
			0.75	2	4	8	24	72	336
Pigment genes (3 of the 33)									
cpcI	8	Phycocyanin synthesis	ns	ns	ns	ns	ns	0.93	0.92
crtO	2	Beta-carotene synthesis	ns	ns	ns	1.05	ns	ns	ns
IPF_1003	16	Beta-carotene synthesis	ns	0.94	0.99	ns	ns	ns	ns
Photosystem genes (0 of the 31)									
C metabolism genes (2 of the 38)									
zwf	6	Glycolysis and oxidative pentose phosphate pathway	ns	ns	ns	0.90	ns	ns	ns
icd	6	Citric acid cycle	ns	ns	ns	0.95	ns	ns	ns
C storage genes (4 of the 15)									
phaC	5	Polyhydroxyalkanoate storage	ns	ns	ns	1.13	ns	ns	ns
phaA	5	Polyhydroxyalkanoate storage	ns	ns	ns	1.18	ns	ns	ns
phaB	5	Polyhydroxyalkanoate storage	ns	ns	ns	1.15	ns	ns	ns
phaE	5	Polyhydroxyalkanoate storage	ns	ns	0.91	1.20	ns	ns	ns
N assimilation genes (9 of the 29)									
glnN	1	GS/GOGAT	ns	1.24	1.51	0.94	ns	1.16	1.45
gltB	1	GS/GOGAT	ns	ns	ns	0.91	ns	ns	ns
nrtA	14	Nitrate transport	ns	1.08	1.02	ns	ns	ns	ns
nrtB	14	Nitrate transport	ns	0.99	ns	ns	ns	ns	ns
ntcB	1	Nitrate transport	ns	1.05	0.90	ns	ns	ns	ns
nirA	1	Nitrite reductase	ns	0.92	ns	ns	ns	ns	ns
IPF_1263	14	Ammonium transport	ns	1.15	1.44	0.97	ns	ns	ns
urtA	14	Urea transport	ns	ns	0.94	ns	ns	ns	ns
IPF_5363	14	Urea transport	ns	0.91	1.01	ns	ns	ns	ns
Stress-related genes (7 of the 22)									
flv2	15	Flavoprotein	ns	ns	-1.81	ns	ns	ns	ns
flv4	15	Flavoprotein	ns	ns	-2.31	ns	ns	ns	ns
isiA	8	Chlorophyll-binding	ns	ns	-1.47	-1.33	ns	ns	-1.76
isiB	8	Flavodoxin	ns	ns	-1.03	ns	ns	ns	ns
sigB	12	Sigma factor	ns	ns	ns	ns	ns	-1.16	ns
sigE	12	Sigma factor	ns	ns	ns	0.94	ns	ns	ns
sigH	12	Sigma factor	ns	ns	-1.30	-1.36	-1.59	-2.49	-2.62

[a]IPF numbers are the locus tags of *Microcystis* PCC 7806 in the EMBL database (AM778843-AM778958).

[b]Gene function categories (CyanoBase): (1) amino acid biosynthesis, (2) biosynthesis of cofactors, prosthetic groups and carriers, (5) central intermediary metabolism, (6) energy metabolism, (8) photosynthesis and respiration, (12) transcription, (14) transport and binding proteins, (15) other categories, (16) hypothetical.

[c]GS/GOGAT: glutamine synthetase/glutamine-2-oxoglutarate amidotransferase.

[d]Log2 values quantify gene expression at the given time point (after increasing the pCO_2) with respect to gene expression at $t = 0$ (just before increasing the pCO_2). Only the responsive genes are shown; the complete data set including all nonresponsive genes is provided in Table S3.4, Supplementary Information. ns: not significant.

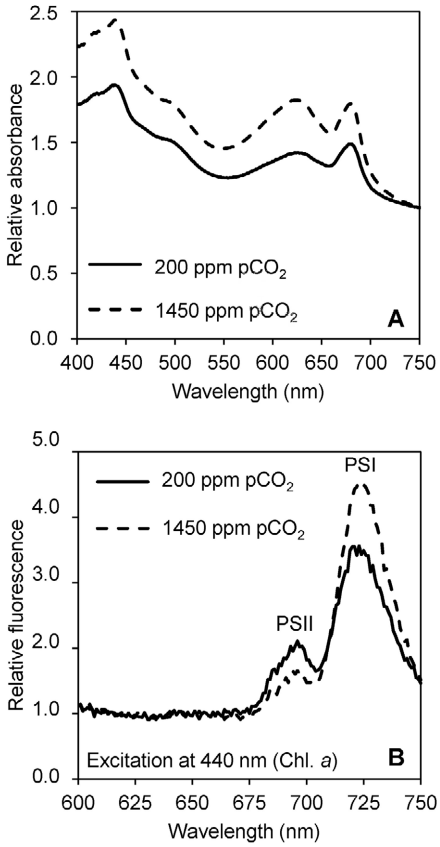

Figure 3.3 Light absorption and emission spectra of cells grown at low pCO_2 (200 ppm) and high pCO_2 (1450 ppm). (A) Light absorption spectra normalized at 750 nm, with peaks of chlorophyll *a* (436 and 678 nm), β-carotene (shoulder at 490 nm) and phycocyanin (626 nm). **(B)** 77K fluorescence emission spectra normalized based on the mean emission at 600-660 nm, with peaks of PSI (695 nm) and PSII (720 nm). The spectra are the average of four biological replicates.

Secondary metabolites including toxins

The microcystin concentration stabilized at ~300 µg L^{-1} at low pCO_2 and increased six-fold to ~2,000 µg L^{-1} at high pCO_2 (**Figure 3.4A**). The microcystin content per cell was ~15 fg $cell^{-1}$ at the steady state at low pCO_2, and increased to ~38 fg $cell^{-1}$ at high pCO_2. Other secondary metabolites produced by *Microcystis* PCC 7806 include aeruginosin, microcyclamide, cyanopeptolin and polyketides. However, expression of the microcystin, aeruginosin, microcyclamide and cyanopeptolin operons did not change significantly (**Figure 3.4B**). In contrast, the expression of two polyketide synthase operons (PKS I/III) increased strongly 72 and 336 h after increasing the pCO_2.

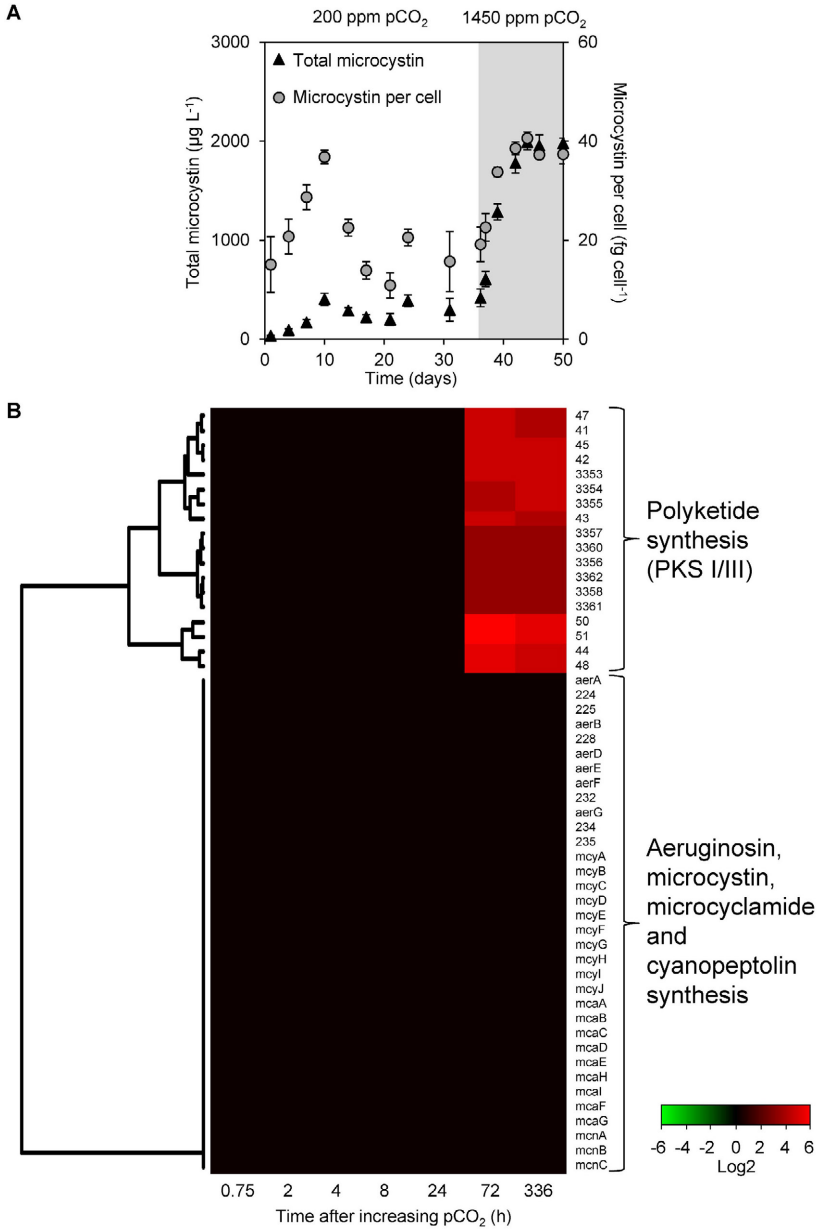

Figure 2.4. Changes in microcystin concentration and gene expression of secondary metabolite genes. (A) Total microcystin concentration and microcystin content per cell, during the shift from low pCO_2 (200 ppm, *white area*) to high pCO_2 (1450 ppm, *shaded area*). Error bars indicate standard deviations (n = 4). **(B)** Changes in expression of the secondary metabolite genes after the increase of pCO_2 to 1450 ppm. Expression changes are quantified as log2 values. Red indicates significant upregulation and green significant downregulation; non-significant changes are in black. Hierarchical clustering was used to order the genes. The underlying data are presented in Table S3.4, Supplementary Information.

Carbon, nitrogen and stress-related genes

Several but not all genes involved in the CCM of Microcystis responded to elevated CO_2 (**Figure 3.5**). Expression of the *cmpABCD* operon encoding the BCT1 bicarbonate uptake system and the *bicA-nhaS3* operon encoding the BicA bicarbonate uptake system was strongly reduced after 2 h at high pCO_2 and remained low during the next 2 weeks. Expression levels of the transcriptional regulators *ccmR* (upstream of the high-affinity CO_2 uptake operon) and *ccmR2* (upstream of the *bicA-nhaS3* operon) were also downregulated at elevated pCO_2. In contrast, expression of the CO_2 uptake genes remained unchanged, except for a slight downregulation of the *ndhF3* gene involved in high-affinity CO_2 uptake. Expression of genes for carboxysome formation (*ccmK2-4*, *ccmL*, *cmmM*, *ccmN* and *ccmO*), RuBisCO (*rbcL*, *rbcS* and *rbcX*) and carbonic anhydrases (*ccaA*, *ecaA* and *ecaB*) remained constant as well (**Figure 3.5**). Results of the microarray experiments were validated with RT-qPCR for selected CCM genes, which gave similar results (**Figure S3.3, Supplementary Information**).

Only a few genes involved in C metabolism and N assimilation showed significant changes in expression at elevated pCO_2 (**Table 3.1**). Expression of *glnN*, encoding for a glutamine synthetase, was upregulated at elevated pCO_2. The genes *nrtA* and *nrtB* involved in nitrate uptake, *nirA* involved in nitrite reduction, and *ntcB* involved in the control of N assimilation were slightly upregulated shortly after increasing the pCO_2.

Several stress-related genes were downregulated at elevated pCO_2, including the flavodiiron protein genes *flv2* and *flv4*, the iron-stress chlorophyll-binding protein gene *isiA* and the sigma factor *sigH* (**Table 3.1**).

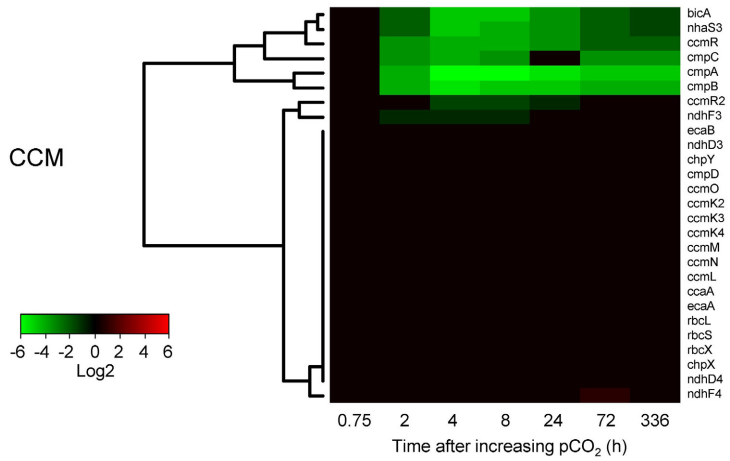

Figure 3.5. Changes in expression of the CO_2-concentrating mechanism (CCM) genes after the increase of pCO_2 to 1450 ppm. Expression changes are quantified as log2 values. Red indicates significant upregulation and green significant downregulation; non-significant changes are in black. Hierarchical clustering was used to order the genes. The underlying data are presented in Table S3.4, Supplementary Information.

Physiological assay of C_i uptake

To assess the activity of the bicarbonate uptake systems BicA and BCT1, O_2 evolution was studied as a function of bicarbonate availability (**Figure 3.6A**). We added 25 mmol L^{-1} NaCl to enable sodium-dependent bicarbonate uptake by BicA. The experiments were performed at pH 9.8, at which DIC contains only ~0.03% CO_2(aq). Without DIC in the medium the samples did not evolve O_2, but their O_2 evolution resumed after addition of $NaHCO_3$. Cells from the chemostats at 200 ppm pCO_2 had a higher affinity at low $NaHCO_3$ concentrations (5-100 µmol L^{-1}) than cells from the chemostats at 1450 ppm pCO_2. At higher $NaHCO_3$ concentrations (300-10,000 µmol L^{-1}), cells from both pCO_2 conditions reached a plateau in O_2 evolution (**Figure 3.6A**). These results suggest that the high-affinity bicarbonate uptake system BCT1 was active in the chemostats at low pCO_2 (200 ppm) but not at elevated pCO_2 (1450 ppm), while the low-affinity bicarbonate uptake system BicA was active at both pCO_2 levels.

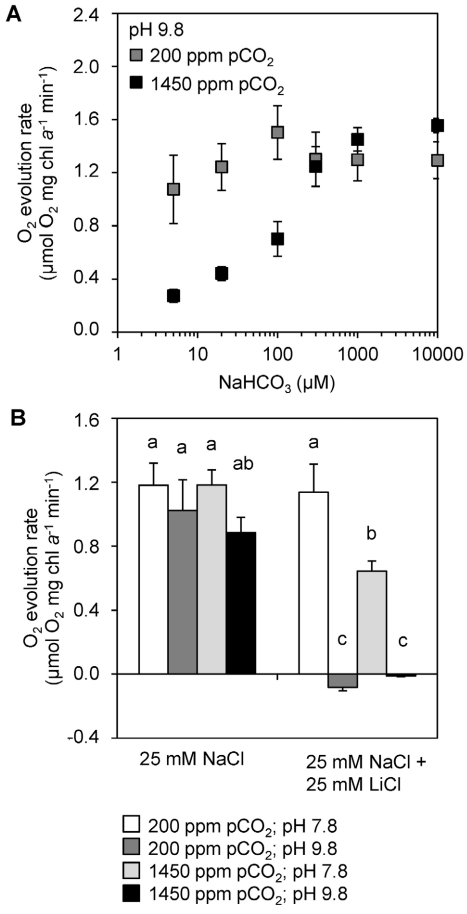

Figure 3.6. Inorganic carbon uptake kinetics of cells grown at low pCO_2 (200 ppm) and high pCO_2 (1450 ppm). (A) Bicarbonate response curves (O_2 evolution rates) of cells grown at low versus high pCO_2 after addition of different concentrations of $NaHCO_3$ at pH 9.8. **(B)** O_2 evolution rates in the presence and absence of LiCl, at pH 7.8 and pH 9.8. The cells were provided with 200 µmol L^{-1} $KHCO_3$. Lithium ions block sodium-dependent bicarbonate uptake, while differences in pH produce different concentrations of CO_2(aq) and bicarbonate. Error bars indicate standard deviations (n = 4). Bars with different letters were significantly different, as tested by a one-way analysis of variance with *post hoc* comparison of the means (α = 0.05).

To further explore the involvement of the C_i uptake systems, we added lithium ions to inhibit the sodium-dependent bicarbonate uptake of BicA (**Figure 3.6B**). These experiments were performed at pH 7.8 and pH 9.8, at which DIC contains 3.7% and 0.03% CO_2(aq), respectively. For cells taken from both low and high pCO_2 chemostats, we found high activity at pH 7.8 and at pH 9.8. However, addition of 25 mmol L^{-1} LiCl resulted in high activity at pH 7.8 but not at pH 9.8. At pH 7.8, the conversion of bicarbonate to CO_2 and subsequent uptake by the CO_2 uptake systems likely compensated for the inactivation of BicA by lithium ions. In contrast, at pH 9.8, when CO_2(aq) is negligible and C_i uptake relies on bicarbonate, the inactivation of BicA by lithium ions was not compensated and drastically reduced C_i uptake. These results suggest that, in the chemostats, both BicA and the CO_2 uptake systems were active at both pCO_2 conditions.

Discussion

Alleviation from C_i limitation

During dense blooms in eutrophic and hypertrophic lakes, cyanobacterial growth can become limited by a low C_i availability (Ibelings and Maberly, 1998; Balmer and Downing, 2011; Verspagen *et al.*, 2014b). Our experiments show that at low atmospheric pCO_2 levels, the photosynthetic activity of the cyanobacteria depleted the CO_2(aq) concentration to the nanomolar range, while the bicarbonate and carbonate concentrations were orders of magnitude higher, which forced cells to primarily use bicarbonate as carbon source. An increase in pCO_2 shifted the growth conditions from very low CO_2(aq) concentrations and modest light availability to higher CO_2(aq) concentrations but lower light levels (**Figure 3.1**). The *Microcystis* population in our experiments benefited strongly from the increased CO_2(aq) availability, and accelerated cell division during the subsequent transient phase. This demonstrates that growth was indeed C_i limited at low pCO_2 levels. The increased cyanobacterial abundance reduced light availability, until the cyanobacterial population settled at a new steady state. Hence, our experiments support the prediction (Verspagen *et al.*, 2014b) that rising CO_2 levels will alleviate cyanobacteria from C_i limitation, and are likely to increase the cyanobacterial abundance in eutrophic and hypertrophic lakes.

Surprisingly, the increase in pCO_2 induced changes in the expression of only 234 genes of *Microcystis* PCC 7806 (**Figure S3.4, Supplementary Information**). This is only ~5% of the total number of protein-encoding genes investigated in this study, and many of these showed differential expression at only a few time points. For instance, only 0.6% of the genes were differentially expressed at the time point of 24 h after the rise in CO_2. In contrast, in other studies, 20-25% of the genes of *Synechocystis* PCC 6803 (Eisenhut *et al.*, 2007) and 50-

55% of the genes of *Synechococcus elongatus* PCC 7942 (Schwarz *et al.*, 2011) were differentially expressed after 24 h of C_i limitation.

The much stronger transcriptome response in these two latter studies than in our results might be explained by differences in experimental design. Eisenhut *et al.* (2007) and Schwarz *et al.* (2011) exposed the cells to C_i starvation, which ceased cell growth and induced a large stress response. In contrast, the growth rate in our chemostat experiments was kept relatively high, which resulted in a milder response to elevated CO_2. An alternative explanation might be that the cyanobacterium *Microcystis* shows a much more specific transcriptome response to changing C_i conditions than *Synechocystis* and *Synechococcus*. *Microcystis* is a buoyant cyanobacterium that can develop dense blooms in eutrophic lakes, where it is typically exposed to a wide range of different CO_2 conditions (Verspagen *et al.*, 2014b). A highly specific transcriptome response that mainly targets the C_i uptake systems could preserve energy and offer a robust strategy for a species that often experiences strongly fluctuating C_i conditions.

Changes in expression of CCM genes

Our results show that the bicarbonate uptake genes encoding for BCT1 and BicA were downregulated at elevated pCO_2 (**Figure 3.5**). Additionally, expression of the transcriptional regulator *ccmR2*, located upstream of the *bicA-nhaS3* operon, was lowered.

BCT1 has a relatively high affinity for bicarbonate ($K_{0.5}$ ~10-15 µmol L^{-1}) and a low flux rate (Omata *et al.*, 2002). In line with expectation, expression of the genes *cmpABCD* encoding BCT1 was highest at the low pCO_2 condition. This is further supported by the bicarbonate response curves of the O_2 optode experiments, which showed high-affinity bicarbonate uptake at low pCO_2 but not at high pCO_2 (**Figure 3.6A**). The high activity of BCT1 in low pCO_2 conditions is consistent with previous studies with other cyanobacteria, which showed enhanced expression of the *cmpABCD* genes upon induction of C_i limitation (Woodger *et al.*, 2003; Eisenhut *et al.*, 2007; Schwarz *et al.*, 2011).

Conversely, BicA has a relatively low affinity for bicarbonate ($K_{0.5}$ ~70-350 µmol L^{-1}) while it has a high flux rate (Price *et al.*, 2004). Contrary to expectation, the *bicA* expression was highest at low pCO_2, where the bicarbonate concentration was only ~60 µmol L^{-1} (**Figure 3.1B**). This was also observed in a study of *Synechococcus* PCC 7002, where the expression of *bicA* was enhanced by C_i limitation (Woodger *et al.*, 2007). However, it differs from studies of *Synechocystis* PCC 6803, which found that the expression of *bicA* was not much affected by the pCO_2 level (Wang *et al.*, 2004; Eisenhut *et al.*, 2007). Our results show that, even though the *bicA* gene of *Microcystis* PCC 7806 was less expressed at high pCO_2, the BicA enzyme was still active at high pCO_2. This is apparent from the O_2 optode experiments in which we blocked

BicA activity with lithium ions (**Figure 3.6**). Hence, BicA appears active at a relatively wide range of bicarbonate concentrations.

Compared to several other *Microcystis* strains, *Microcystis* PCC 7806 lacks the bicarbonate uptake system SbtA (Sandrini *et al.*, 2014), which has an even higher affinity for bicarbonate ($K_{0.5}$ < 2 µmol L^{-1}) than BCT1 (Price *et al.*, 2004). Therefore, *Microcystis* PCC 7806 seems less adapted to very low bicarbonate conditions than SbtA-containing *Microcystis* strains, and was likely trying to take up as much bicarbonate as possible by expressing both BCT1 and BicA at the low pCO_2 condition, even though the BicA uptake system did not operate very efficiently at that stage.

In contrast to the strong response of the bicarbonate uptake genes, gene expression of the CO_2 uptake systems was not affected by elevated pCO_2 (**Figure 3.5**). For instance, the *chpX* and *chpY* genes, encoding for the CO_2 hydration subunit of the low-affinity and high-affinity CO_2 uptake systems, respectively, were constitutively expressed in *Microcystis* PCC 7806. The constitutive expression of *chpX* is consistent with studies of other cyanobacteria (Woodger *et al.*, 2003; Wang *et al.*, 2004; Schwarz *et al.*, 2011). However, the constitutive expression of *chpY* contrasts with studies of other cyanobacteria, which found that *chpY* was highly inducible when cells were exposed to C_i limitation (Price *et al.*, 2004; Wang *et al.*, 2004; Schwarz *et al.*, 2011). Constitutive expression of the CO_2 uptake systems indicates that at low CO_2(aq) concentrations the *Microcystis* cells were still capable of CO_2 uptake. This was confirmed by the O_2 optode experiments, which showed that CO_2 uptake was active at both pCO_2 levels when bicarbonate uptake was blocked by lithium ions (**Figure 3.6B**).

Expression of the transcriptional regulator *ccmR*, located upstream of the high-affinity CO_2 uptake operon, was strongly downregulated at high pCO_2 (**Figure 3.5**). This is noteworthy, because expression of the high-affinity CO_2 uptake genes did not respond to elevated pCO_2. Possibly, CcmR regulates the expression of the *cmpABCD* operon of *Microcystis*, which was strongly downregulated at high pCO_2. This would be consistent with the observation that CmpR, a known transcriptional regulator of the *cmpABCD* operon in other cyanobacteria, is lacking in *Microcystis* (Sandrini *et al.*, 2014). Indeed, Woodger *et al.* (2007) previously showed that CcmR in *Synechococcus* PCC 7002 does not only control the high-affinity CO_2 uptake operon but also the expression of other CCM genes.

Interestingly, gene expression of several key components of the CCM, including carboxysome, RuBisCO and carbonic anhydrase genes, was not affected by elevated pCO_2 (**Figure 3.5**), suggesting that cells did not alter carboxysome component numbers. This is counterintuitive, since C_i availability strongly increased after the upshift in pCO_2. Yet, it seems that *Microcystis* simply adjusted its C_i uptake arsenal to deal with the change in C_i availability. In contrast, studies that induced C_i limitation in *Synechocystis* PCC 6803 and *Synechococcus*

elongatus PCC 7942 observed downregulation of carboxysomal genes after 24 h (Eisenhut *et al.*, 2007; Schwarz *et al.*, 2011). Possibly, the cyanobacteria in these latter studies did not need to produce new carboxysomes, because their growth rate was arrested in the experiments of Eisenhut *et al.* (2007) and Schwarz *et al.* (2011). This differs from our chemostat experiments, in which the growth rate was kept relatively high by the dilution rate, and hence carboxysome production should be maintained. Therefore, differences in experimental design might explain these results. Alternatively, the contrasting results might reflect species-specific differences, where *Microcystis* displays a milder response to fluctuating C_i conditions than these other cyanobacteria (see preceding discussion).

Reduced expression of stress-related genes

Our results show reduced expression of several stress genes (*flv2*, *flv4*, *isiA* and *sigH*) at elevated CO_2 (**Table 3.1**). Flavodiiron proteins have previously been linked to acclimation to low C_i conditions (Zhang *et al.*, 2009, Allahverdiyeva *et al.*, 2011; Bersanini *et al.*, 2014). Flv2 and Flv4 are unique for cyanobacteria. They are involved in photoprotection of the PSII complex (Zhang *et al.*, 2009), and can function as electron sink (Bersanini *et al.*, 2014). Reduced expression of the flavodiiron protein genes *flv2* and *flv4* at elevated pCO_2 is in agreement with previous studies with *Synechocystis* PCC 6803 (Wang *et al.*, 2004; Eisenhut *et al.*, 2007).

The iron-stress chlorophyll-binding protein IsiA can function as a storage unit for spare chlorophyll molecules, as a PSI antenna enhancing the light harvesting ability, and in addition can protect PSII from photooxidative stress (Yeremenko *et al.*, 2004; Havaux *et al.*, 2005). Reduced expression of the *isiA* gene at elevated pCO_2 likely signifies lower levels of oxidative stress, which shifted the IsiA-bound spare chlorophylls to new chlorophyll protein complexes.

Sigma factors are involved in transcription initiation. Expression of *sigH* typically increases with general stress (Huckauf *et al.*, 2000; Hakkila *et al.*, 2013). The expression of *sigH* was lowered in our study after the increase in pCO_2 (**Table 3.1**), indicating that the cells perceived less stress at this stage.

Increased toxins per cell at elevated CO_2?

Our results show that cells of *Microcystis* PCC 7806 contained a 2.5 times higher microcystin content at elevated pCO_2. Similar results were found in an earlier study with *Microcystis* HUB 5-2-4, where elevated CO_2 also produced a transition from C_i to light limitation and an approximately 2-2.5 fold increase in microcystin content (Van de Waal *et al.*, 2009). This suggests that rising CO_2 levels will increase the toxicity of *Microcystis* cells.

In contrast to the increase of the cellular microcystin content, expression of the *mcy* genes remained constant during the shift from low pCO_2 to high pCO_2 (**Figure 3.4B**). Gene expression may not be equivalent to abundance of the final gene product, and a further complication is that microcystins are synthesized by non-ribosomal peptide synthetases (Dittmann *et al.*, 1997). The control mechanisms for the synthetase activity are largely unknown, but it has been suggested that amino acid availability may play a decisive role (Tonk *et al.*, 2008; Van de Waal *et al.*, 2010a).

The microarray results showed a strong increase in two polyketide synthase operons (PKS I/III) at elevated pCO_2 (**Figure 3.4B**). These operons were described previously (Frangeul *et al.*, 2008; Makower *et al.*, 2015), yet the structure of the actual produced compounds and their exact function remain unknown. Polyketides have diverse biological functions and many have pharmacological and toxicological properties. Further research is needed to know more about the polyketides of cyanobacteria.

Other physiological responses to elevated CO_2

Our results also point at several other physiological changes in response to rising pCO_2 levels. For example, the dry weight of cells decreased ~2 fold at elevated pCO_2, but the cells were hardly smaller (**Figure 3.2A**). This was accompanied by a reduced cellular C storage, lower cellular C/N ratio and reduced carbohydrate content at elevated pCO_2 (**Figure 3.2B-D**). A lower cellular C content at elevated CO_2 contradicts the common expectation that rising CO_2 levels will increase the carbon content of phytoplankton cells (*e.g.*, Van de Waal *et al.*, 2010b; Finkel *et al.*, 2010; Verschoor *et al.*, 2013). However, recent experiments showed that also other *Microcystis* strains do not increase their C/N ratio at elevated CO_2 when provided with an ample nutrient supply (Verspagen *et al.*, 2014a). A possible explanation for these observations might be that cells do not require large amounts of C reserves in the presence of plentiful C_i in the environment. Furthermore, changes in carbohydrate content are known to play a role in the vertical migration of *Microcystis* (Thomas and Walsby, 1985; Visser *et al.*, 1997; Wallace *et al.*, 2000). A strong decrease in cellular dry matter and carbohydrate content will increase the buoyancy of cells, which may be particularly advantageous when cells experience low light levels. The shift from C_i to light limitation induced by rising CO_2 concentrations may thus stimulate the formation of surface blooms in *Microcystis*-dominated lakes.

Elevated pCO_2 levels also led to an increase in the photosynthetic pigments and in the PSI/PSII ratio of the cells (**Figure 3.3A,B**). Most likely, this response is due to the reduced light availability caused by the denser cultures at elevated pCO_2. This process, known as photoacclimation, is well known to occur in cyanobacteria (Deblois *et al.*, 2013). Yet, expression of the psa and psb genes for photosystem components remained unaltered.

We did not observe many changes in the genes involved in C and N metabolism (**Table 3.1**). One exception is the upregulation of *glnN*, that encodes for a glutamine synthase. The expression of *glnN* has been linked with nitrogen stress (Reyes *et al.*, 1997). In this way the N metabolism of the cells responds subtly to changes in C_i availability caused by high pCO_2 levels.

Concluding remarks

We investigated the genetic and physiological response of the harmful cyanobacterium *Microcystis* to rising CO_2. The experiments were conducted in chemostats, which provide ideal conditions to study microorganisms in a controlled environment. Yet, chemostats provide a simplified experimental setting in comparison to the complexity of the natural world. In lakes, buoyancy regulation enables *Microcystis* populations to form dense blooms at the water surface (Reynolds and Walsby, 1975; Huisman *et al.*, 2004), where they intercept the influx of atmospheric CO_2 (Ibelings and Maberly, 1998). Hence, the formation of surface blooms is a successful strategy to avoid low CO_2 availability deeper in the water column (Paerl and Ustach, 1982). However, despite their proximity to the surface, dissolved CO_2 concentrations can be strongly depleted and pH may exceed 9 during surface blooms of buoyant cyanobacteria (López-Archilla *et al.*, 2004; Verspagen *et al.*, 2014b). The high concentration of cells in blooms causes a high local demand for inorganic carbon and consequently extreme carbon limitation (Ibelings and Maberly, 1998), resembling the conditions in our CO_2-limited laboratory experiments.

In our experiments, elevated CO_2 alleviated *Microcystis* cells from C_i limitation. In response, *Microcystis* induced changes in the expression of a relatively limited number of genes, including several genes involved in C_i uptake. The expression of several stress-related genes was reduced at elevated CO_2, while only a few key genes at control sites of cellular C/N metabolism were regulated. At elevated CO_2, *Microcystis* cells halted its high-affinity bicarbonate uptake systems, and relied on CO_2 and low-affinity bicarbonate uptake systems. This supports earlier results that high-affinity bicarbonate uptake systems will become less essential with rising CO_2 (Sandrini *et al.*, 2014). This may ultimately lead to an evolutionary loss of high-affinity C_i uptake systems, as shown in evolution experiments with the green alga *Chlamydomonas reinhardtii*. This green alga lost its ability to induce high-affinity C_i uptake while maintaining its low-affinity C_i uptake after 1,000 generations at elevated CO_2 levels (Collins and Bell, 2004; Collins *et al.*, 2006).

In addition to changes in C_i uptake, elevation of the CO_2 concentrations in our experiments also led to a higher population abundance, increased buoyancy of the cells, and higher toxin content per *Microcystis* cell. This indicates that the current rise in atmospheric

CO_2 levels may strongly increase the problems associated with the harmful cyanobacterium *Microcystis* in eutrophic lakes.

Materials and Methods

Chemostat experiment

The axenic strain *Microcystis* strain PCC 7806 was obtained from the Pasteur Culture Collection (Paris, France). The strain was originally isolated from the Braakman reservoir, the Netherlands in 1972. It contains genes for the two CO_2 uptake systems, the bicarbonate uptake systems BCT1 (high affinity) and BicA (low affinity), but lacks the high-affinity bicarbonate uptake system SbtA (Sandrini *et al.*, 2014). The *Microcystis* strain was pre-cultured in four 2-L Erlenmeyer flasks using modified BG11 medium (Rippka *et al.*, 1979) with 10 mmol L^{-1} $NaNO_3$ and without Na_2CO_3 or $NaHCO_3$, at an incident light intensity of 15 µmol photons m^{-2} s^{-1}, 400 ppm CO_2, and a temperature of 25°C. Regular microscopy did not reveal contaminations.

The experiment was carried out in four replicate chemostats designed for phytoplankton growth (Huisman *et al.*, 2002) using the same modified BG11 medium. Each chemostat consisted of a flat culture vessel that was illuminated from one side (the front surface) to obtain a unidirectional light gradient. We applied a constant incident irradiance (I_{in}) of 50 µmol photons m^{-2} s^{-1} using white fluorescent tubes (Philips Master TL-D 90 De Luxe 18W/965, Philips Lighting, Eindhoven, the Netherlands). The chemostats had an optical path length of 5 cm and an effective working volume of 1.8 L. The temperature in the chemostats was maintained at 25°C using a stainless steel cooling finger connected to a water bath (Haake A28F/AC200; Thermo Fisher Scientific, Pittsburgh, PA, USA). The dilution rate was set at 0.01 h^{-1}.

The chemostats were bubbled with CO_2-enriched air at a flow rate of 25 L h^{-1}. The CO_2-enriched air was based on pressurized air (21% O_2, 78% N_2), from which the CO_2 was removed by a CO_2 adsorption air dryer (Ecodry K-MT6; Parker Zander, Lancaster, NY, USA) and four 1 m high columns filled with NaOH pellets. Subsequently, different amounts of pure CO_2 gas were added using GT 1355R-2-15-A 316 SS Flow Controllers and 5850S Mass Flow Controllers (Brooks Instrument, Hatfield, PA, USA) to obtain the desired CO_2 concentration. The gas mixture was moistened with 25°C water to suppress evaporation and led through a 0.20 µm Midisart 2000 filter (Sartorius Stedim Biotech GmbH, Göttingen, Germany) to sterilize the air, before it entered the chemostats. The CO_2 concentration in the gas mixture was checked regularly with an Environmental Gas Monitor for CO_2 (EGM-4; PP Systems, Amesbury, MA, USA).

Prior to the experiment, the four chemostats were inoculated with *Microcystis* from exponentially growing pre-cultures. The cultures were allowed to acclimate to the new chemostat conditions for ten days. Subsequently, the cultures were diluted to an initial cyanobacterial abundance of ~60 mm^3 L^{-1} to start the experiment. The CO_2 concentration in the gas mixture was 200±10 ppm CO_2 during the first 36 days of the experiment (and also during the preceding acclimation phase). After 36 days, the CO_2 concentration was raised to 1450±50 ppm CO_2. The experiment was run for 50 days, during which the chemostats were sampled three to five times per week.

Light and cyanobacterial abundance

The incident irradiance (I_{in}) and the irradiance penetrating through the chemostat vessel (I_{out}) were measured with a LI-COR LI-250 quantum photometer (LI-COR Biosciences, Lincoln, NE, USA) at ten positions on the front and back surface of the chemostat vessels, respectively. Cell numbers, biovolumes and average cell size of samples were determined in triplicate using a Casy 1 TTC cell counter with a 60 µm capillary (Schärfe System GmbH, Reutlingen, Germany). Dry weight was determined in duplicate by filtering 0.75-10 mL of sample over pre-weighted 1.2 µm pore size 25 mm GF/C glass filters (Whatman GmbH, Dassel, Germany). Filters with cells were dried for two days in a 60°C oven, transferred to a desiccator to cool to room temperature, and subsequently weighted again.

Aquatic chemistry

The pH of the samples was measured immediately after sample collection with a Lab 860 pH meter in combination with a BlueLine 28 Gel pH electrode (SCHOTT Instruments GmbH, Mainz, Germany). For dissolved inorganic carbon (DIC) concentration, alkalinity and nitrate measurements, samples of 40 mL were immediately centrifuged (5 min at 4,000 *g* and 20°C). The pellets were used for cellular C and N analysis, whereas the supernatant was filtered over 0.45 µm pore size 47 mm polyethersulfone membrane filters (Sartorius AG, Goettingen, Germany). The filtrate was transferred to sterile plastic urine tubes (VF-109SURI; Terumo Europe N.V., Leuven, Belgium). The tubes were filled completely and stored at 4°C until further analysis. DIC (three to five technical replicates) was measured with a TOC-VCPH TOC analyzer (Shimadzu, Kyoto, Japan). Concentrations of CO_2(aq), bicarbonate and carbonate were calculated from DIC and pH (Stumm and Morgan, 1996). Alkalinity was determined with a 716 DMS Titrino titrator (Metrohm Applikon B.V., Schiedam, the Netherlands), based on the amount of 0.01 or 0.1 mol L^{-1} HCl added to reach pH 4.5 (ISO 9963-1:1994). The nitrate concentration was measured with a TNM-1 nitrogen detector (Shimadzu, Kyoto, Japan) attached to the TOC-VCPH TOC analyzer.

Cellular composition

Cellular C and N contents were determined by gently washing the pellets obtained from the previous centrifugation twice (5 min at 4,000 *g* and 20°C) with a C- and N-free solution (10 mmol L^{-1} NaCl and 10 mmol L^{-1} K_2HPO_4 pH 8.0). The washed pellets were stored at -20°C until further analysis. Subsequently, the pellets were freeze dried, and the C and N content of 5 mg homogenized freeze-dried powder was analyzed using a Vario EL Elemental Analyzer (Elementar Analysensysteme GmbH, Hanau, Germany).

To determine the cellular carbohydrate, lipid, protein and phosphate content, 2 mL samples were centrifuged and the pellets were stored at -20°C until further analysis. Carbohydrate was quantified using the phenol-sulphuric acid method, with D-glucose (Merck Millipore, Darmstadt, Germany) as standard (Dubois *et al.*, 1956). Lipids were extracted with methanol and chloroform, and subsequently the lipid content was quantified using the sulphuric acid-vanillin-phosphoric acid method, with Triolein (>99%, Sigma-Aldrich Co, St Louis, MO, USA) as standard (Izard and Limberger, 2003). Proteins were quantified with the Bradford assay, using Brilliant Blue G-250 and bovine serum albumin as standard (Bradford, 1976). Cellular P was obtained by oxidizing cells with potassium persulfate for 1 h at 100°C (Wetzel and Likens, 2000), after which the phosphate concentration was measured colorimetrically according to Murphy and Riley (1962).

In vivo absorption spectra

Light absorption spectra of the samples were scanned from 400 to 750 nm with a bandwidth of 0.4 nm using an Aminco DW-2000 double-beam spectrophotometer (Olis Inc., Bogart, GA, USA). BG11 medium without cells was used as baseline and the spectra were normalized based on the absorbance at 750 nm.

Low temperature fluorescence

Relative amounts of PSI and PSII were determined using an Olis DM 45 77K spectrofluorometer connected to an Olis photon counter (Olis Inc., Bogart, GA, USA). Glycerol (30% final concentration) was added to the samples, which were transferred to 3 mL polystyrene cuvettes (Sigma-Aldrich Co, St Louis, MO, USA) and frozen in liquid nitrogen. The excitation wavelength was 440 nm for chlorophyll *a*. Emission spectra of the samples were measured in triplicate at 600-750 nm, and normalized based on the mean emission at 600-660 nm.

Microcystin analysis

Microcystis PCC 7806 produces two microcystin variants, [Asp3]MC-LR and MC-LR (Tonk *et al.*, 2009). To determine the intracellular unbound microcystin content (*cf.* Meissner *et al.*, 2013), 1-5 mL samples were filtered over 1.2 µm pore size 25 mm GF/C filters (Whatman GmbH, Dassel, Germany). The filters were stored at -20°C and subsequently freeze dried. Microcystins were extracted with 75% MeOH and analysed with HPLC according to Van de Waal *et al.* (2011), using a Shimadzu LC-20AD HPLC system with a SPD-M20A photodiode array detector (Shimadzu, Kyoto, Japan). Peaks of [Asp3]MC-LR and MC-LR could not be completely separated. Therefore, both peaks were summed and are referred to as total microcystin. Earlier chemostat experiments showed that extracellular microcystin concentrations in the water phase were negligible (*e.g.*, Van de Waal *et al.*, 2011).

RNA extraction

RNA samples for transcriptome analysis were taken from all four chemostats, at 0 hours (just before increasing the pCO_2) and at 0.75, 2, 4, 8, 24, 72 and 336 h after increasing the pCO_2 from 200 to 1450 ppm. Fresh culture samples of ~40 mL were immediately cooled on ice and centrifuged for 5 min at 4,000 *g* and 4°C in a pre-cooled centrifuge. The pellets were immediately resuspended in 1 mL TRIzol (Life Technologies, Grand Island, NY, USA), frozen in liquid nitrogen and stored at -80 °C. Subsequently, RNA was extracted with TRIzol (Invitrogen) according to the supplier's instructions, using beads (0.5 mm BashingBeads; Zymo Research, Orange, CA, USA) to facilitate cell disruption. After the phase separation steps, the Direct-ZolTM RNA MiniPrep kit (Zymo Research) was used for RNA purification. The in-column DNase I digestion was included as well. RNA concentrations were quantified using a Nanodrop 1000 spectrophotometer (Thermo Scientific, San Jose, CA, USA), and all RNA samples had A_{260}/A_{280} and A_{260}/A_{230} values above 1.8. The quality of the RNA extracts was checked using an Agilent 2100 Bioanalyzer (Agilent Technologies, Amstelveen, the Netherlands).

cDNA synthesis for microarray analysis

The cDNA library was prepared using the Superscript III Reverse Transcriptase kit (Invitrogen, Carlsbad, CA, USA) according to Eisenhut *et al.* (2007), with incorporation of Cy3-dUTP or Cy5-dUTP (Amersham Biosciences Benelux, Roosendaal, the Netherlands) in the cDNA. Non-incorporated fluorescent nucleotides were removed with the QIAquick PCR purification kit (Qiagen, Venlo, the Netherlands). The reverse transcription and fluorescent dye incorporation efficiency were monitored with a Nanodrop 1000 spectrophotometer (Thermo Scientific, San Jose, CA, USA).

Microarray design

The transcriptome study was performed on two Agilent 8×60K two-color microarray chips (Agilent Technologies, Amstelveen, the Netherlands). The microarray design and probe library of *Microcystis* PCC 7806 was based on Makower *et al.* (2015), which was partly derived from Straub *et al.* (2011). The sequence-specific oligonucleotide probes (60-mers) targeted 4,691 protein-coding genes, which corresponds to 88.6% of the total predicted protein-coding genes in the annotated genome of *Microcystis* PCC 7806 (Frangeul *et al.*, 2008). On average, five different probes per gene were used. Cy3- and Cy5-labeled cDNA probe samples from just before and at specific time points after increasing the pCO_2 in the four chemostats were combined. A loop design was used, in which samples from the same chemostat but different time points were compared (**Table S3.1**). The hybridization, washing and array reading were performed as described by Eisenhut *et al.* (2007).

Microarray data analysis

The array data were analyzed with the R package Limma version 3.18.13 (Smyth, 2005; www.bioconductor.org; www.R-project.org). After background correction ('minimal method'), within-array normalization was applied using global loess normalization. Subsequently, the data was log2 transformed. Between-array normalization was applied using A-quantile normalization (Bolstad *et al.*, 2003). Log2 expression values for the different time points (after increasing the pCO_2) were calculated with respect to the reference value at $t = 0$ (just before increasing the pCO_2). Expression values of multiple probes per gene were averaged. Hence, for each gene we obtained four expression values per time point, based on the four replicate chemostats. For each time point, *p*-values were calculated from the moderated *t*-statistic, and were adjusted for multiple hypothesis testing by controlling the false discovery rate (Storey and Tibshirani, 2003). Log2 gene expression values of < -0.9 or > 0.9 (similar to Nodop *et al.*, 2008 and Schwarz *et al.*, 2011), and *p*-values < 0.01 were considered differentially expressed. Visual representation was done using hierarchical clustering and heatmaps with the hclust and heatmap.2 functions of the R gplots package version 2.13.0. The expression values, corresponding *p*-values and gene function according to CyanoBase (http://genome.microbedb.jp/cyanobase/Synechocystis/genes/category) of all investigated genes are listed in **Table S3.2, Supplementary Information**.

RT-qPCR gene expression analysis

To validate the microarray results, we also investigated changes in gene expression of several CCM genes and the *mcyB* gene using RT-qPCR. We designed gene-specific primers (**Table S3.3, Supplementary Information**). Secondary structure analysis of the primers was checked

with OligoAnalyzer 3.1 (Integrated DNA Technologies, Coralville, IA, USA) and the *in silico* specificity was assessed using Primer-BLAST (Ye *et al.*, 2012). The specificity of the primers was confirmed with normal PCR on genomic DNA using the GoTaq® Hot Start DNA polymerase kit (Promega GmbH, Mannheim, Germany) combined with gel electrophoresis.

For the RT-qPCR gene expression analysis, we used the same RNA samples as for the microarray analysis at the time points 0 h, 4 h and 336 h (2 weeks) after increasing the pCO_2. cDNA was synthesized by reverse transcription of the RNA samples with Superscript III (Invitrogen) according to the supplier's instructions, using 250 ng random hexamers (Amersham Biosciences Benelux, Roosendaal, the Netherlands) and 5 µg of pure RNA in a total reaction volume of 20 µL. Next, the RNase H treatment (New England Biolabs, Ipswich, MA, USA) was applied to remove any RNA complementary to the cDNA. Subsequently, the qPCR Maxima® SYBR Green Master Mix (2x) (Thermo Fisher Scientific, Pittsburgh, PA, USA) was applied on the cDNA samples according to the supplier's instructions, in an ABI 7500 Real-Time PCR system (Applied Biosystems, Foster City, CA, USA). The two step cycling protocol was used, with a denaturation temperature of 95°C (15 s) and a combined annealing/extension temperature of 60°C (60 s) during 40 cycles. The reactions contained 0.3 µmol L^{-1} primers and 1 µL of 10 times diluted cDNA from the RT reaction in a total reaction volume of 25 µL. Other reaction components were added as instructed by the supplier. ROX solution was used to correct for any well-to-well variation and melting curve analysis was performed on all measured samples to rule out non-specific PCR products.

Amplification efficiencies of individual runs (*E*) were calculated with LinRegPCR (version 2012.3; Ramakers *et al.*, 2003; Ruijter *et al.*, 2009) and were between 1.8 and 2.0 (**Table 3.3**). Time point 0 (just before the pCO_2 was increased) was used as reference sample, and 16S rRNA was used as reference gene. Each RT-qPCR plate contained a reference sample and samples with primers targeting 16S rRNA to overcome plate effects. For each individual sample, two technical replicates were measured and the average of the two measurements was used in the data analysis. The data were baseline corrected using LinRegPCR, and the same software was used to calculate quantification cycle (*Cq*) values. LinRegPCR did not detect samples without amplification, without a plateau, with a baseline error or noise error, or with deviating amplification efficiencies. Negative control samples did not show significant amplification. For each gene, we calculated the relative gene expression with respect to time point 0 using 16S rRNA as reference gene according to the $2^{-\Delta\Delta Ct}$ method (Livak and Schmittgen, 2001). MS Excel version 2010 and SPSS version 20.0 were used for the statistical analyses. A one-tailed *t*-test was used to assess whether the change in gene expression with respect to time point 0 was significant (again with $n = 4$ expression values per time point, based on the four replicate chemostats). An independent samples *t*-test was used to detect differences

between the 4 h and 2 week samples. The false discovery rate (FDR) was used to correct for multiple hypothesis testing (Benjamini and Yekutieli, 2001; FDR adjusted p values<0.05).

O_2 optode experiments

In mineral medium without nitrate, the O_2 evolution rate of cyanobacterial cells exposed to saturating light provides a good proxy of their C_i uptake rate (Miller *et al.*, 1988). We therefore measured O_2 evolution with an Oxy-4 mini O_2 optode (PreSens GmbH, Regensburg, Germany) to study the C_i uptake of samples from the steady-state chemostats at 200 and 1450 ppm pCO_2. External carbonic anhydrase activity in *Microcystis* was previously shown to be negligible (Song and Qiu, 2007). Fresh cell samples were pelleted (4,000 *g* for 5 min at 20°C), washed 1x and then resuspended in C_i- and nitrate-depleted modified BG11 medium (no added $NaNO_3$ and $NaCO_3$/$NaHCO_3$, but with 25 mmol L^{-1} NaCl and 10 mmol L^{-1} CAPSO-NaOH added at pH 9.8; the medium was aerated with N_2 gas for 4h before usage). The absorbance at 750 nm (A_{750}) of washed and resuspended samples was 0.300. Three mL of sample was inserted into custom-made glass incubation chambers (four measurements were done at the same time), each connected to an O_2 optode. The glass chambers were connected to a RM6 water bath (Lauda, Lauda-Königshofen, Germany) to keep the temperature of the samples at 20.3°C. Magnetic stirring was used for mixing. The O_2 optode sensors were calibrated with N_2 gas ('0%') and air ('100%'). A saturating amount of light (500 µmol photons m^{-2} s^{-1}) was used, which was provided by KL1500 compact Schott lamps (Schott AG, Mainz, Germany). Subsequently, specific amounts of $NaHCO_3$ were added (5, 20, 100, 300, 1000 or 10,000 µmol L^{-1}), after which the rate of O_2 evolution (µmol L^{-1} min^{-1}) was measured. The evolution was expressed per mg of chlorophyll *a*. Photosynthetic pigments were extracted with 90% acetone and analyzed using HPLC with photodiode array detection (LC-20AD liquid chromatographs, SIL-20A auto sampler, CTO-20AC column oven, SPD-M20A diode array detector, RF-10AXL fluorescence detector; Shimadzu, Kyoto, Japan). Identification of chlorophyll *a* was based on the characteristic absorbance at 664 nm and the specific retention time compared with a standard obtained from DHI Group (Copenhagen, Denmark).

To evaluate the activity of the different C_i uptake systems, we investigated O_2 evolution in the presence and absence of 25 mmol L^{-1} LiCl. Lithium ions are known to inhibit the activity of the sodium-dependent bicarbonate uptake systems (*e.g.*, Espie *et al.*, 1988). The experiments were performed at pH 7.8 (using 10 mmol L^{-1} TES-KOH pH 7.8 buffer) and pH 9.8 (using 10 mmol L^{-1} CAPSO-KOH pH 9.8 buffer) to vary the relative availability of CO_2 and HCO_3^-, using C_i and N depleted modified BG11 medium containing 25 mmol L^{-1} NaCl to which 200 µmol L^{-1} $KHCO_3$ was added after initial C_i depletion. To test if O_2 evolution rates differed significantly between the treatments, one-way analysis of variance was used with

post hoc comparison of the means based on Tukey's test (n = 4 replicates per treatment).

Acknowledgements

We thank the reviewers for their helpful comments on the manuscript, Pieter Slot for assistance with the HPLC measurements, Leo Hoitinga for assistance with the TOC-VCPH analyzer, and Chiara Cerli for assistance with the Elemental Analyser. We thank the MicroArray Department (MAD) of the University of Amsterdam for support with the microarray hybridization and scanning, and especially Floyd Wittink for assistance in the array design. This research was supported by the Division of Earth and Life Sciences (ALW) of the Netherlands Organization for Scientific Research (NWO). J.M. Schuurmans acknowledges support by the BE-BASIC Foundation. J. Huisman acknowledges support from the Turner-Kirk Charitable Trust for his stay at the Isaac Newton Institute for Mathematical Sciences of the University of Cambridge.

Supplementary Information

Contents

This section contains the following data:

I. Supplementary Figures

II. Supplementary Tables

I. Supplementary Figures

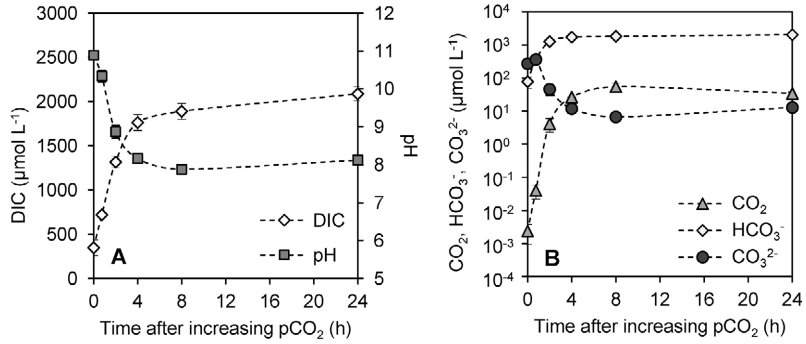

Figure S3.1. Changes in inorganic carbon chemistry and pH during the first 24 h after increasing the pCO_2. (A) Dissolved inorganic carbon (DIC) and pH. **(B)** Dissolved CO_2, bicarbonate and carbonate concentrations. Error bars indicate standard deviations (n = 4).

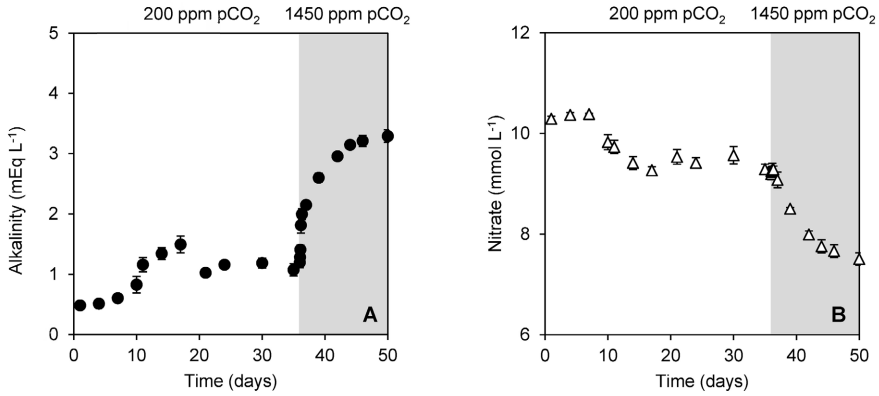

Figure S3.2. Changes in alkalinity and nitrate concentration during the shift from low pCO_2 (200 ppm, white area) to high pCO_2 (1450 ppm, shaded area). (A) Alkalinity. **(B)** Nitrate concentration. Error bars indicate standard deviations (n = 4).

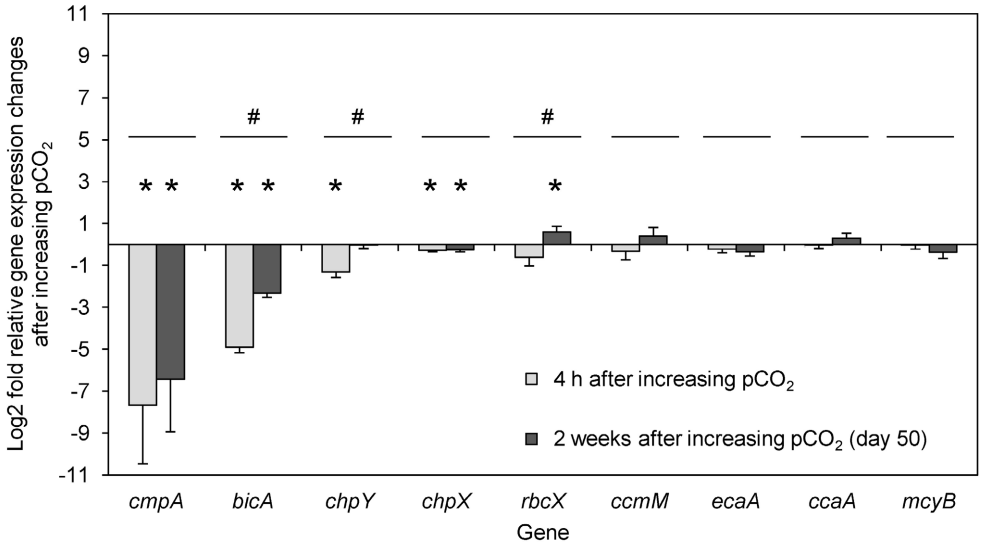

Figure S3.3. Changes in gene expression of CCM genes and the microcystin gene *mcyB* assessed with RT-qPCR, at 4 h and 2 weeks after the shift from low pCO_2 (200 ppm) to high pCO_2 (1450 ppm). Error bars indicate standard deviations (n = 4). * significantly different (p < 0.05) from the zero time point (200 ppm). # significant difference (p < 0.05) between the time points of 4 h and 2 weeks after the increase to 1450 ppm. The p-values were corrected for multiple hypothesis testing.

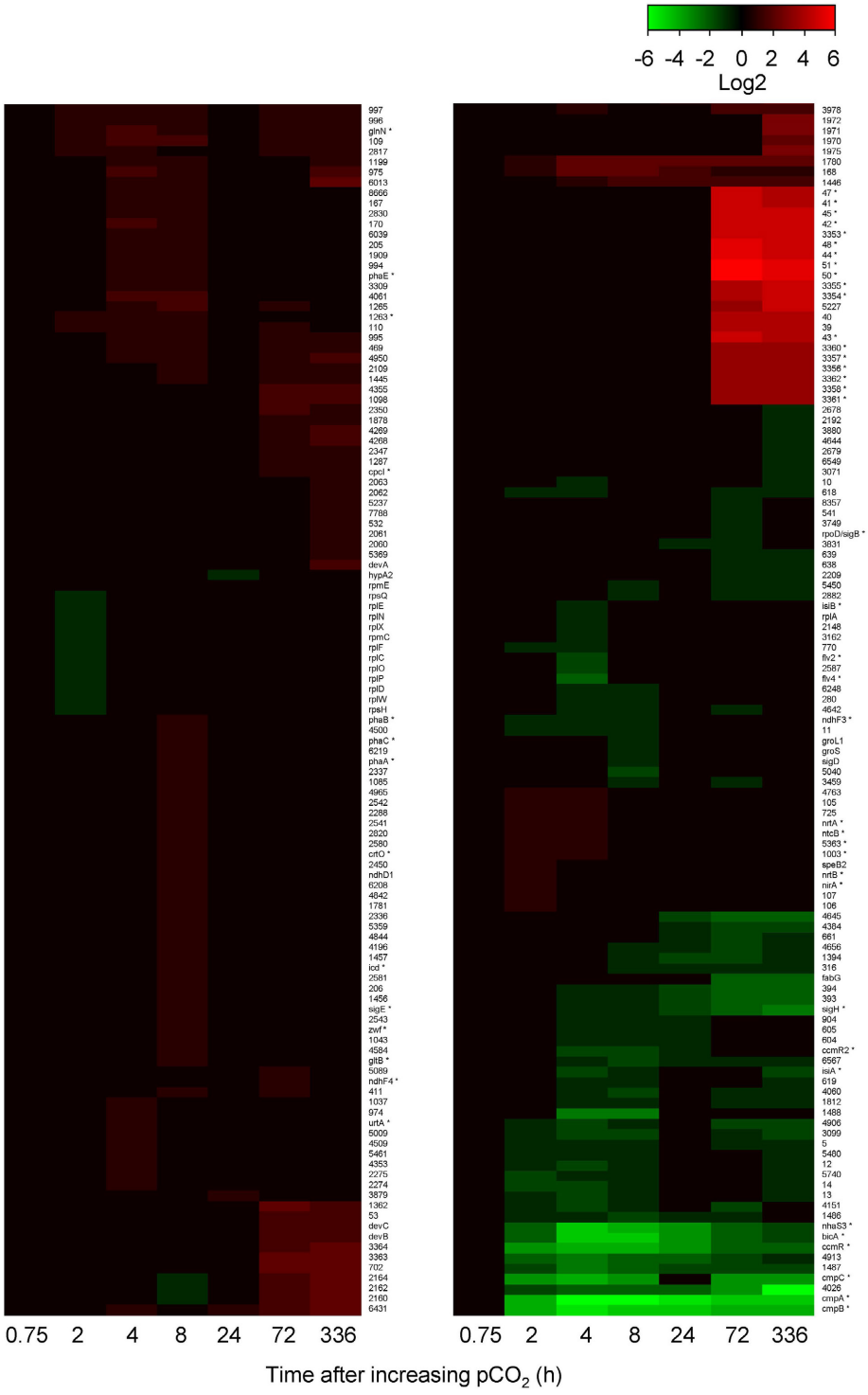
-6 -4 -2 0 2 4 6
Log2
997
996
glnN *
109
2817
1199
975
6013
8666
167
2830
170
6039
205
1909
994
phaE *
3309
4061
1265
1263 *
110
995
469
4950
2109
1445
4355
1098
2350
1878
4269
4268
2347
1287
cpcI *
2063
2062
5237
7788
532
2061
2060
5369
devA
hypA2
rpmE
rpsQ
rplE
rplN
rplX
rpmC
rplF
rplC
rplO
rplP
rplD
rplW
rpsH
phaB *
4500
phaC *
6219
phaA *
2337
1085
4965
2542
2288
2541
2820
2580
ortO *
2450
ndhD1
6208
4842
1781
2336
5359
4844
4196
1457
icd *
2581
206
1456
sigE *
2543
zwf *
1043
4584
gltB *
5089
ndhF4 *
411
1037
974
urtA *
5009
4509
5461
4353
2275
2274
3879
1362
53
devC
devB
3364
3363
702
2164
2162
2160
6431
3978
1972
1971
1970
1975
1780
168
1446
47 *
41 *
45 *
42 *
3353 *
48 *
44 *
51 *
50 *
3355 *
3354 *
5227
40
39
43 *
3360 *
3357 *
3356 *
3362 *
3358 *
3361 *
2678
2192
3880
4644
2679
6549
3071
10
618
8357
541
3749
rpoD/sigB *
3831
639
638
2209
5450
2882
isiB *
rplA
2148
3162
770
flv2 *
2587
flv4 *
6248
280
4642
ndhF3 *
11
groL1
groS
sigD
5040
3459
4763
105
725
nrtA *
ntcB *
5363 *
1003 *
speB2
nrtB *
nirA *
107
106
4645
4384
661
4656
1394
316
fabG
394
393
sigH *
904
605
604
ccmR2 *
6567
isiA *
619
4060
1812
1488
4906
3099
5
5480
12
5740
14
13
4151
1486
nhaS3 *
bicA *
ccmR *
4913
1487
cmpC *
4026
cmpA *
cmpB *
0.75 2 4 8 24 72 336
0.75 2 4 8 24 72 336
Time after increasing pCO_2 (h)

Figure S3.4. Overview of all genes responding to rising pCO_2. The expression changes are shown as log2 values. Red indicates significant upregulation and green significant downregulation; non-significant changes are in black. Hierarchical clustering was used to order the genes. Genes with superscript * are also shown in the main text. The complete data set can be found in Table S3.2, Supplementary Information.

II. Supplementary Tables

Table S3.1. Microarray chip loading scheme.

Sample ID[a]	Biological replicate	Chip	Array	Dye	Slide side
t0	1	1	3	Cy5	R
t0	2	1	4	Cy3	R
t0	3	2	11	Cy3	R
t0	4	2	12	Cy5	R
t0.75	1	1	1	Cy5	R
t0.75	2	1	2	Cy3	R
t0.75	3	2	9	Cy3	R
t0.75	4	2	10	Cy5	R
t2	1	1	5	Cy3	L
t2	2	1	4	Cy5	R
t2	3	2	13	Cy5	L
t2	4	2	12	Cy3	R
t4	1	1	3	Cy3	R
t4	2	1	2	Cy5	R
t4	3	2	11	Cy5	R
t4	4	2	10	Cy3	R
t8	1	1	5	Cy5	L
t8	2	1	6	Cy3	L
t8	3	2	13	Cy3	L
t8	4	2	14	Cy5	L
t24	1	1	7	Cy3	L
t24	2	1	6	Cy5	L
t24	3	2	15	Cy5	L
t24	4	2	14	Cy3	L
t72	1	1	7	Cy5	L
t72	2	1	8	Cy3	L
t72	3	2	15	Cy3	L
t72	4	2	16	Cy5	L
t336	1	1	1	Cy3	R
t336	2	1	8	Cy5	L
t336	3	2	9	Cy5	R
t336	4	2	16	Cy3	L

[a]The samples ID's indicate the time after increasing the pCO_2.

Table S3.2. Complete transcriptome data.

The complete transcriptome data are provided in the Supplementary Material of Sandrini *et al.* (2015a). *Frontiers in Microbiology* **6:** 401. doi: 10.3389/fmicb.2015.00401.

Table S3.3. *Microcystis* primers used in the RT-qPCR gene expression analysis.

Primer name	Sequence 5'→ 3' (length)	Gene symbol	Locus tag	Accession no. (Genbank)	Expected product size (bp)	Amplification efficiency (*E*)[a]	Reference
16S rRNA-F	GTCGAACGGGAATCTTCGGAT (21)	16S rRNA	*IPF_5548*	AM778951.1	132	1.88±0.03	This study
16S rRNA-R	GCTAATCAGACGCAAGCTCTTC (22)						This study
bicA-F	CAAGCTAACGGTCGCATCAT (20)	*bicA*	*IPF_4911*	AM778949.1	157	1.87±0.02	This study
bicA-R	AGGCACATCACTCAAGTCCA (20)						This study
cmpA-F	GTTAAACACCCAGGGTAACGGA (22)	*cmpA*	*IPF_2181*	AM778958.1	180	1.85±0.01	This study
cmpA-R	GCTAACCAGTAACGAATCCAGAAGT (25)						This study
chpX-F	CCTGTCAAGTCCTCCTCTCAT (21)	*chpX*	*IPF_1842*	AM778957.1	113	1.89±0.01	This study
chpX-R	TTCAGGATACCCACTACCTCG (21)						This study
chpY-F	ATATCGCCAAAATGCCGACC (20)	*chpY*	*IPF_1545*	AM778958.1	114	1.80±0.02	Sandrini *et al.*, 2014
chpY-R	GACATCATCCGCACCTGTTC (20)						Sandrini *et al.*, 2014
rbcX-F	CGGATCATGACGGTAAGAGAACA (23)	*rbcX*	*IPF_2531*	AM778933.1	157	1.85±0.02	This study
rbcX-R	ATTCCGATGTCTCTGGTTGACT (22)						This study
ccmM-F	AAGTCCACACCTTCTCTAACCTC (23)	*ccmM*	*IPF_5695*	AM778933.1	118	1.87±0.01	Sandrini *et al.*, 2014
ccmM-R	CTGTCGTCGCCAATGTGAA (19)						Sandrini *et al.*, 2014
ccaA-F	ACTCCTGCGGTTAATACTGTGG (22)	*ccaA*	*IPF_5538*	AM778919.1	97	1.87±0.01	Sandrini *et al.*, 2014
ccaA-R	GATAAATGCGATCAGCTTGGGAG (23)						Sandrini *et al.*, 2014
ecaA-F	CCCAAGAACCTTCTCCTGAAATG (23)	*ecaA*	*IPF_4566*	AM778932.1	187	1.86±0.01	Sandrini *et al.*, 2014
ecaA-R	GCCAATTGTTGCAGTTGTTGG (21)						Sandrini *et al.*, 2014
mcyB-F	ATCCCATGCTCAGAGACGTT (20)	*mcyB*	*IPF_375*	AM778952.1	163	1.88±0.01	Sandrini *et al.*, 2014
mcyB-R	AGATGTCCGCAGGGATTCAT (20)						Sandrini *et al.*, 2014

[a]The average amplification efficiency (*E*) ± s.d. of 12-36 samples for each primer pair was calculated using LinRegPCR (version 2012.3).

Table S3.4. Expression of genes involved in pigment synthesis, photosystems, CCM, C metabolism, C storage, N assimilation, stress response and secondary metabolites.

IPF/gene[a]	IPF[a]	Function category[b]	Annotation	Gene expression changes after increasing pCO_2 (log2 values)[c]						
				t = 0.75	*t* = 2	*t* = 4	*t* = 8	*t* = 24	*t* = 72	*t* = 336
Pigment genes										
chlG	1784	2	Chlorophyll *a* synthesis	-0.041	-0.086	-0.022	0.181	0.340	0.274	0.102
chlL	2403	2	Chlorophyll *a* synthesis	0.182	0.008	-0.285	-0.355	-0.441	0.086	0.243
chlN	2405	2	Chlorophyll *a* synthesis	0.212	0.147	-0.110	-0.123	-0.319	-0.014	0.248
chlB	1478	2	Chlorophyll *a* synthesis	0.162	0.281	-0.032	0.044	-0.131	0.254	0.181
chlH	2836	17	Chlorophyll *a* synthesis	-0.033	-0.027	0.025	-0.198	-0.231	-0.069	0.069
chlI	4936	2	Chlorophyll *a* synthesis	-0.182	-0.207	-0.334	-0.078	0.099	-0.343	-0.574
chlP	4969	2	Chlorophyll *a* synthesis	0.237	0.428	0.167	0.304	-0.038	-0.186	-0.125
acsF	4518	16	Chlorophyll *a* synthesis	0.089	0.256	0.258	0.328	0.021	0.018	-0.165
chlD	4280	2	Chlorophyll *a* synthesis	0.001	0.059	-0.009	0.227	0.393	-0.073	-0.230
chlM	5642	2	Chlorophyll *a* synthesis	-0.042	0.103	0.017	0.051	-0.011	-0.093	-0.246
3758	3758	2	Chlorophyll *a* synthesis	-0.028	0.018	-0.282	-0.025	-0.122	-0.187	-0.515
644	644	8	Phycocyanin synthesis	0.179	0.124	0.183	0.151	0.178	0.216	0.667
apcA	881	8	Phycocyanin synthesis	0.061	0.328	0.223	0.532	0.410	0.572	0.338
apcB1	882	8	Phycocyanin synthesis	-0.067	0.297	0.150	0.453	0.293	0.238	-0.048
apcC	883	8	Phycocyanin synthesis	-0.011	0.188	0.144	0.405	0.339	0.501	0.333
2153	2153	17	Phycocyanin synthesis	-0.004	-0.130	-0.168	0.010	0.033	0.046	0.022
2154	2154	17	Phycocyanin synthesis	0.024	-0.095	-0.122	-0.066	-0.066	-0.052	0.023
2636	2636	17	Phycocyanin synthesis	-0.007	-0.109	-0.068	-0.160	-0.255	-0.110	-0.094
nblB	2775	8	Phycocyanin synthesis	-0.029	-0.016	-0.056	0.044	0.250	0.229	0.266
cpcB	4221	8	Phycocyanin synthesis	0.039	0.216	0.311	0.373	0.259	0.509	0.620
cpcA	4222	8	Phycocyanin synthesis	-0.008	0.229	0.282	0.380	0.264	0.371	0.425
cpcI	4223	8	Phycocyanin synthesis	0.112	0.190	0.293	0.338	0.379	0.926	0.919
cpcF	4758	8	Phycocyanin synthesis	-0.114	-0.222	-0.200	-0.065	0.079	-0.017	-0.125
cpcE	4760	8	Phycocyanin synthesis	-0.208	-0.108	-0.103	0.074	0.240	-0.051	-0.274
crtO	1740	2	Beta-carotene synthesis	0.236	0.444	0.700	1.051	0.359	0.511	0.321
crtQ	5749	2	Beta-carotene synthesis	-0.118	0.011	0.075	-0.209	0.063	-0.024	0.017
crtP1	2974	2	Beta-carotene synthesis	-0.018	-0.056	-0.111	-0.352	0.263	0.178	0.153
crtH	4648	16	Beta-carotene synthesis	0.047	0.034	0.094	-0.065	0.061	0.167	0.242
crtP2	2656	17	Beta-carotene synthesis	-0.061	0.105	0.144	-0.056	-0.072	0.028	-0.009
crtE	4168	2	Beta-carotene synthesis	0.078	-0.027	0.107	0.200	0.379	0.451	0.437
861	861	2	Beta-carotene synthesis	-0.301	-0.211	-0.406	-0.449	-0.290	-0.431	-0.548
1003	1003	16	Beta-carotene synthesis	0.308	0.935	0.989	0.622	0.495	0.292	0.284
4676	4676	2	Beta-carotene synthesis	0.042	0.027	-0.025	0.039	-0.117	0.011	0.112
Photosystem genes										
psaA	474	8	Photosystem I	0.012	0.305	0.193	0.199	-0.044	-0.036	-0.047
psaB	476	8	Photosystem I	-0.193	0.269	0.092	0.116	-0.188	-0.739	-0.978
psaC	3989	8	Photosystem I	0.094	0.426	0.123	0.282	0.053	0.066	0.072
psaD	2761	8	Photosystem I	0.111	0.244	0.266	0.195	0.084	0.280	0.327
psaE	446	8	Photosystem I	0.026	0.411	0.219	0.442	0.219	0.344	0.159
psaF	3393	8	Photosystem I	-0.070	0.199	0.124	0.022	-0.042	0.061	0.002
psaI	2821	8	Photosystem I	0.063	0.353	0.194	0.142	0.010	-0.127	-0.166
psaJ	3392	8	Photosystem I	-0.128	0.183	0.165	-0.009	-0.055	-0.044	-0.134
psaK1	3184	8	Photosystem I	-0.091	0.188	0.014	0.222	-0.042	-0.228	-0.260
psaK2	5244	8	Photosystem I	-0.094	0.351	0.512	0.825	0.424	0.360	0.321
psaL	2822	8	Photosystem I	0.182	0.492	0.357	0.385	0.186	0.352	0.217
psbA1	4371	8	Photosystem II	-0.445	-0.144	-0.278	-0.423	-0.492	-0.714	-0.770
psbA2	868	8	Photosystem II	-0.324	-0.108	-0.195	-0.321	-0.394	-0.468	-0.452
psbV	4990	8	Photosystem II	0.176	0.325	0.342	0.414	0.499	0.536	0.546
psbK	1293	8	Photosystem II	-0.108	-0.021	-0.048	0.149	0.051	-0.349	-0.141
psb27	5583	8	Photosystem II	0.073	-0.041	-0.065	0.233	0.469	0.532	0.544
psbP	2468	8	Photosystem II	0.011	0.011	0.060	0.156	-0.027	0.141	0.228
psb28	4328	8	Photosystem II	-0.181	-0.180	-0.183	-0.015	-0.086	-0.169	-0.137
psbZ	3202	8	Photosystem II	0.075	0.176	0.299	0.149	0.098	0.295	0.430
psbL	5911	8	Photosystem II	-0.038	0.046	-0.066	-0.149	0.042	0.156	0.160
4776	4776	8	Photosystem II	-0.029	0.025	-0.048	-0.135	0.003	0.097	0.239
PsbU	5553	8	Photosystem II	-0.164	0.050	0.039	0.245	0.101	-0.265	-0.317

Table S3.4 continued.

PsbN	5537	8	Photosystem II	0.117	0.082	-0.043	-0.222	-0.211	-0.095	-0.006
psbC	3580	8	Photosystem II	0.009	0.304	0.163	0.143	0.121	-0.176	-0.259
psbD1	3579	17	Photosystem II	0.103	0.195	0.197	-0.032	0.086	0.286	0.336
psbO	4364	8	Photosystem II	-0.057	0.183	0.025	0.140	0.131	-0.145	-0.220
psb29	658	16	Photosystem II	-0.027	-0.195	-0.185	-0.439	0.198	0.202	0.277
psbQ	4959	16	Photosystem II	-0.080	-0.169	-0.020	0.069	0.112	0.114	0.153
psbI	1964	8	Photosystem II	-0.033	0.034	-0.098	-0.153	-0.095	-0.086	-0.055
psbH	1588	8	Photosystem II	-0.068	-0.033	-0.012	-0.065	0.035	-0.047	-0.054
psbW	4806	8	Photosystem II	0.104	0.058	0.065	0.178	0.323	0.326	0.143
CO_2-concentrating mechanism genes										
ndhD4	1459	8	CO_2 uptake	0.179	0.136	0.111	0.313	0.209	0.498	0.483
chpY	1545	8	CO_2 uptake	-0.622	-0.677	-0.780	-0.541	-0.300	-0.200	-0.167
ndhD3	1546	8	CO_2 uptake	-0.729	-0.815	-0.824	-0.583	-0.279	0.013	-0.054
ecaB	1547	8	Carbonic anhydrase	-0.370	-0.362	-0.491	-0.286	-0.038	0.191	0.170
ndhF3	1548	8	CO_2 uptake	-0.902	-1.066	-1.286	-1.053	-0.506	-0.262	-0.342
ccmR	1549	10	Transcriptional regulator	-1.966	-3.207	-4.152	-4.022	-3.479	-2.252	-2.119
chpX	1842	8	CO_2 uptake	-0.087	-0.140	-0.203	-0.134	-0.179	-0.106	-0.086
ccmR2	2166	10	Transcriptional regulator	0.028	-0.794	-1.778	-1.775	-1.055	-0.296	-0.390
cmpD	2177	14	Bicarbonate uptake	-1.508	-1.282	-1.694	-1.406	-1.251	-1.435	-1.510
cmpC	2178	14	Bicarbonate uptake	-2.230	-3.198	-4.119	-3.376	-3.315	-3.374	-3.455
cmpB	2180	14	Bicarbonate uptake	-2.621	-4.187	-5.126	-4.457	-4.396	-4.120	-4.102
cmpA	2181	14	Bicarbonate uptake	-1.904	-3.938	-6.177	-5.793	-5.226	-4.793	-4.650
rbcS	2530	8	RuBisCO subunit	-0.291	-0.312	-0.431	-0.016	0.215	0.044	0.009
rbcX	2531	8	RuBisCO chaperone	-0.268	-0.425	-0.389	-0.097	0.221	0.295	0.316
rbcL	2532	8	RuBisCO subunit	-0.189	-0.365	-0.401	-0.075	0.260	0.372	0.407
ccmN	2533	8	Carboxysome	-0.407	-0.452	-0.453	-0.011	0.245	0.175	0.150
ccmO	3425	8	Carboxysome	-0.155	-0.115	-0.092	0.073	0.151	0.220	0.228
ccmK3	3718	8	Carboxysome	-0.179	-0.200	0.087	0.135	0.273	0.180	0.264
ecaA	4566	8	Carbonic anhydrase	-0.040	-0.105	-0.186	-0.249	-0.177	-0.213	-0.132
bicA	4911	14	Bicarbonate uptake	-0.606	-2.232	-4.532	-4.562	-3.327	-2.171	-1.735
nhaS3	4912	14	Na^+/H^+ antiporter	-0.658	-2.353	-4.460	-4.269	-3.186	-2.270	-1.798
ndhF4	5045	8	CO_2 uptake	0.099	0.030	0.375	0.671	0.892	0.952	0.703
ccmK2	5495	8	Carboxysome	-0.262	-0.248	-0.212	0.059	0.226	0.234	0.248
ccaA	5538	8	Carbonic anhydrase	0.062	-0.058	0.175	0.183	0.351	0.606	0.629
ccmM	5695	8	Carboxysome	-0.364	-0.361	-0.288	0.036	0.231	0.188	0.176
ccmK4	5855	8	Carboxysome	-0.135	-0.194	0.197	0.338	0.456	0.398	0.439
ccmL	6196	8	Carboxysome	-0.282	-0.323	-0.218	0.031	0.205	0.356	0.316
C metabolism genes										
cbbZ	4853	6	C2 cycle	-0.027	0.011	0.065	-0.102	-0.151	0.073	0.067
5105	5105	16	C2 cycle	0.041	0.262	0.245	-0.023	0.202	0.043	0.229
glcD	2797	6	C2 cycle	0.005	-0.099	-0.333	-0.280	-0.182	-0.120	-0.105
glcF	4338	6	C2 cycle	-0.051	-0.109	-0.125	-0.013	0.100	0.023	-0.004
5118	5118	15	C2 cycle	0.019	0.134	-0.145	0.291	-0.058	-0.514	-0.505
glyA	1726	1	C2 cycle	0.144	0.125	-0.243	-0.317	-0.164	-0.030	-0.076
serA	3464	1	C2 cycle	-0.197	-0.048	0.018	0.208	0.017	-0.180	-0.395
ilvG	3465	1	Glycerate pathway	0.089	0.218	0.209	0.132	0.173	0.090	0.318
ilvB	864	1	Glycerate pathway	-0.030	-0.142	-0.204	0.123	0.318	-0.028	-0.147
4195	4195	17	Glycerate pathway	0.069	0.099	0.171	0.233	0.180	0.112	-0.012
cbbR	556	10	Calvin-Benson cycle	0.013	-0.267	-0.281	-0.109	0.120	0.305	0.367
gap2	4508	8	Calvin-Benson cycle	-0.023	0.020	-0.057	-0.104	0.268	0.163	0.144
gap1	2286	6	Calvin-Benson cycle	0.154	0.388	0.341	0.710	-0.264	-0.015	-0.167
pgk	2454	6	Calvin-Benson cycle	-0.108	-0.005	-0.127	-0.021	0.198	-0.094	-0.069
tpi	5206	8	Calvin-Benson cycle	-0.057	-0.178	-0.298	-0.589	0.221	0.178	0.320
zwf	2448	6	Glycolysis and PPP	0.348	0.503	0.760	0.903	-0.019	0.333	0.527
pgi	942	6	Glycolysis and PPP	0.093	0.196	0.301	0.193	0.291	0.495	0.527
pfkA1	2807	6	Glycolysis and PPP	-0.086	0.117	0.167	0.759	-0.053	-0.175	-0.476
4300	4300	6	Glycolysis and PPP	0.150	0.227	0.131	0.483	-0.168	-0.008	-0.086
862	862	6	Glycolysis and PPP	-0.138	0.164	-0.036	-0.171	-0.196	-0.343	-0.521

Table S3.4 continued.

4919	4919	15	Glycolysis and PPP	-0.067	0.214	0.234	0.341	0.247	-0.280	-0.419
eno	6528	6	Glycolysis and PPP	0.078	0.455	0.350	0.517	0.033	-0.158	-0.150
4761	4761	6	Glycolysis and PPP	-0.060	0.061	0.157	0.305	0.425	0.271	0.038
628	628	17	Glycolysis and PPP	0.479	0.364	0.461	0.523	0.104	0.587	0.880
5643	5643	6	Glycolysis and PPP	0.058	0.323	0.626	0.632	-0.069	0.085	0.002
5946	5946	6	Glycolysis and PPP	-0.001	-0.035	-0.114	-0.048	0.029	0.074	0.147
665	665	6	Glycolysis and PPP	-0.089	-0.015	0.043	0.036	0.075	-0.020	-0.080
4658	4658	6	Glycolysis and PPP	-0.193	-0.174	-0.443	-0.259	-0.132	-0.319	-0.546
nifJ	4303	8	Glycolysis and PPP	0.319	0.454	0.274	0.717	-0.317	-0.002	-0.187
ppc	1728	6	Glycolysis and PPP	-0.096	0.113	0.409	0.334	0.165	0.042	0.167
5068	5068	17	Glycolysis and PPP	0.131	0.443	0.738	0.848	-0.043	0.033	-0.073
2629	2629	6	Glycolysis and PPP	0.092	0.316	0.110	-0.004	0.029	0.047	-0.179
gltA	4674	6	Citric acid cycle	0.371	0.607	0.774	0.880	-0.144	0.097	0.177
acnB	5675	15	Citric acid cycle	0.071	0.218	0.027	-0.168	-0.307	-0.383	-0.265
icd	1980	6	Citric acid cycle	0.147	0.434	0.639	0.955	-0.026	0.165	-0.009
fumC	4474	6	Citric acid cycle	0.011	0.169	0.231	0.145	-0.026	-0.308	-0.226
sdhA	5037	6	Citric acid cycle	0.254	0.441	0.282	0.886	-0.008	-0.218	-0.467
sdhB	5962	6	Citric acid cycle	0.125	0.190	0.048	0.293	-0.141	-0.060	-0.136
C storage genes										
phaC	4967	5	Polyhydroxyalkanoate	0.304	0.581	0.856	1.132	-0.027	0.299	0.197
phaA	4962	5	Polyhydroxyalkanoate	0.469	0.783	0.888	1.176	-0.019	0.452	0.273
phaB	4963	5	Polyhydroxyalkanoate	0.367	0.675	0.899	1.150	0.041	0.404	0.256
phaE	4966	5	Polyhydroxyalkanoate	0.349	0.665	0.911	1.204	-0.033	0.320	0.143
glgP2	2422	5	Starch/glycogen	0.046	0.344	0.213	0.517	-0.386	-0.423	-0.368
glgP1	5378	5	Starch/glycogen	0.058	0.217	0.506	0.899	-0.162	0.184	0.041
glgB	1591	5	Starch/glycogen	-0.084	-0.036	-0.047	-0.134	-0.095	-0.088	-0.040
3632	3632	5	Starch/glycogen	0.033	0.026	0.113	0.420	0.065	0.057	0.106
glgA2	3726	5	Starch/glycogen	-0.257	-0.201	-0.411	-0.696	-0.209	-0.037	0.043
glgA1	5358	5	Starch/glycogen	-0.249	-0.095	-0.020	0.097	0.121	-0.048	-0.155
glgC	112	5	Starch/glycogen	0.031	0.117	0.045	0.067	0.203	0.228	0.268
623	623	16	Starch/glycogen	0.166	0.088	-0.112	0.058	0.172	0.194	0.268
1564	1564	6	Sucrose synthesis	0.137	-0.048	-0.606	-0.578	-0.768	-0.882	-0.865
1565	1565	17	Sucrose synthesis	0.103	-0.112	-0.426	-0.496	-0.663	-0.649	-0.596
1566	1566	6	Sucrose synthesis	0.073	-0.013	-0.282	-0.341	-0.530	-0.556	-0.544
N assimilation genes										
gcvT	3351	6	Gly cleavage system	-0.112	0.005	0.035	0.165	0.213	0.075	0.053
gcvP	5353	6	Gly cleavage system	-0.036	0.031	-0.220	-0.436	-0.198	-0.338	-0.376
gcvH	4892	6	Gly cleavage system	-0.330	-0.175	0.124	0.192	0.353	0.127	-0.109
phdD	4856	6	Gly cleavage system	-0.072	-0.047	-0.132	-0.031	-0.032	-0.061	-0.076
glnA	3887	1	GS/GOGAT	0.236	0.553	0.495	0.595	-0.170	-0.025	-0.037
glnN	5525	1	GS/GOGAT	1.092	1.240	1.510	0.937	0.637	1.164	1.448
gltB	3409	1	GS/GOGAT	0.290	0.399	0.419	0.913	0.113	0.398	0.104
glsF	4630	1	GS/GOGAT	-0.086	-0.125	-0.277	-0.245	-0.080	-0.219	-0.309
nrtA	2949	14	Nitrate transport	0.743	1.082	1.023	0.344	0.346	0.591	0.757
nrtB	2950	14	Nitrate transport	0.738	0.992	0.882	0.418	0.360	0.618	0.823
ntcB	535	1	Nitrate transport	0.861	1.054	0.902	0.516	0.570	0.797	0.722
nirA	3545	1	Nitrite reductase	0.765	0.921	0.806	0.348	0.326	0.496	0.849
5474	5474	14	Ammonium transport	-0.090	0.047	0.059	-0.021	-0.010	-0.135	0.002
5724	5724	17	Ammonium transport	0.083	0.240	0.196	0.026	-0.091	-0.145	0.041
1263	1263	14	Ammonium transport	0.498	1.147	1.438	0.968	0.818	0.586	0.463
ureG	2471	5	Urease encoding genes	-0.123	-0.164	-0.089	0.002	-0.045	-0.300	-0.195
ureC	2853	5	Urease encoding genes	-0.052	0.265	0.469	0.711	0.414	0.393	0.112
ureB	6535	5	Urease encoding genes	0.067	0.038	0.091	0.101	0.106	0.307	0.135
ureA	6536	5	Urease encoding genes	0.046	0.037	0.085	0.062	0.064	0.221	0.157
ureD	592	5	Urease encoding genes	-0.105	-0.231	-0.360	-0.307	-0.167	-0.188	-0.114
ureF	1116	5	Urease encoding genes	0.002	-0.005	-0.072	-0.182	-0.069	-0.074	-0.023
ureE	3586	5	Urease encoding genes	0.131	0.137	0.013	-0.004	-0.046	-0.029	0.245
urtA	5362	14	Urea transport	0.331	0.834	0.941	0.706	0.466	0.407	0.244
5363	5363	14	Urea transport	0.545	0.907	1.008	0.822	0.625	0.848	0.790

Table S3.4 continued.

5364	5364	14	Urea transport	0.407	0.754	0.856	0.657	0.469	0.666	0.604
urtD	5366	14	Urea transport	0.345	0.672	0.865	0.562	0.441	0.667	0.523
urtE	5367	14	Urea transport	0.321	0.616	0.847	0.598	0.432	0.580	0.489
cynS	869	1	Other	0.344	0.436	0.324	0.133	0.292	0.512	0.316
narB	1469	1	Other	0.503	0.586	0.387	0.160	0.221	0.500	0.542
Stress-related genes										
flv1	2831	17	Flavoprotein	-0.060	-0.101	-0.066	-0.097	0.013	0.122	0.141
flv2	2588	15	Flavoprotein	-1.425	-1.372	-1.806	-1.556	-1.601	-1.028	-1.024
flv3	5216	17	Flavoprotein	0.072	0.278	0.239	-0.100	-0.066	0.095	0.281
flv4	2586	15	Flavoprotein	-1.871	-1.616	-2.307	-2.078	-2.020	-1.621	-1.632
sodB1	3451	17	Other	-0.019	-0.034	0.258	0.488	0.563	0.710	0.550
sodB2	4715	4	Other	0.048	0.076	0.135	0.066	0.206	0.190	0.333
1-cys prx	5966	15	Other	0.034	0.190	0.346	0.867	-0.098	0.121	-0.071
2-cys prx	1847	4	Other	-0.172	-0.286	-0.337	-0.596	-0.107	-0.382	-0.273
tII prx	5431	15	Other	-0.341	-0.626	-0.737	-0.139	0.603	0.180	-0.080
prxQB1	2514	14	Other	-0.062	-0.054	0.016	0.269	-0.005	-0.051	-0.174
prxQB2	4076	14	Other	-0.103	-0.149	-0.376	-0.422	-0.293	-0.414	-0.352
prxQB3	3971	17	Other	-0.060	-0.038	-0.256	-0.518	-0.142	-0.377	-0.405
isiA(C242)	5322	8	Other	-0.452	-0.452	-1.467	-1.329	-1.062	-1.116	-1.757
isiA(C305)	4218	8	Other	-0.432	-0.560	-1.550	-1.238	-0.998	-1.110	-1.740
isiB	4217	8	Other	-0.227	-0.385	-1.034	-0.838	-0.669	-0.718	-0.857
sigA	4798	12	Sigma factor	0.151	0.358	0.447	0.294	-0.037	0.077	0.318
sigB	2772	12	Sigma factor	-0.145	-0.041	-0.024	-0.638	-0.869	-1.158	-0.860
sigD	6533	12	Sigma factor	-0.174	-0.172	-0.526	-0.966	-0.614	-0.804	-0.778
sigE	5730	12	Sigma factor	0.415	0.809	0.835	0.937	-0.069	0.256	0.351
sigF	5732	12	Sigma factor	0.130	-0.165	0.388	0.299	0.252	0.649	0.858
sigG	5143	12	Sigma factor	-0.083	0.254	0.262	0.009	-0.091	-0.259	-0.073
sigH	392	12	Sigma factor	-0.109	-0.630	-1.299	-1.360	-1.591	-2.489	-2.621
Secondary metabolite										
41	41	17	Polyketide synthesis (I/III)	0.806	-0.305	0.501	-0.747	-0.316	4.628	4.242
42	42	17	Polyketide synthesis (I/III)	0.844	-0.286	0.581	-0.794	-0.301	4.835	4.364
43	43	17	Polyketide synthesis (I/III)	0.776	-0.214	0.514	-0.781	-0.416	4.389	4.026
44	44	16	Polyketide synthesis (I/III)	0.895	-0.322	0.530	-0.953	-0.308	5.261	4.761
45	45	17	Polyketide synthesis (I/III)	0.734	-0.437	0.393	-0.973	-0.399	4.855	4.376
47	47	17	Polyketide synthesis (I/III)	0.801	-0.317	0.331	-0.853	-0.123	4.667	4.175
48	48	17	Polyketide synthesis (I/III)	0.902	-0.263	0.432	-1.036	-0.057	5.091	4.748
50	50	15	Polyketide synthesis (I/III)	1.089	-0.031	0.470	-1.133	0.512	5.804	5.359
51	51	17	Polyketide synthesis (I/III)	1.076	0.109	0.487	-1.068	0.573	5.464	5.045
3353	3353	17	Polyketide synthesis (I/III)	0.550	-0.694	0.476	-0.111	0.213	4.515	4.820
3354	3354	17	Polyketide synthesis (I/III)	0.678	-0.682	0.168	-0.262	0.064	4.182	4.566
3355	3355	17	Polyketide synthesis (I/III)	0.683	-0.681	0.286	-0.230	0.031	4.052	4.376
3356	3356	17	Polyketide synthesis (I/III)	0.735	-0.374	0.274	-0.140	0.099	3.416	3.576
3357	3357	17	Polyketide synthesis (I/III)	0.763	-0.311	0.285	-0.068	0.133	3.358	3.580
3358	3358	17	Polyketide synthesis (I/III)	0.721	-0.350	0.204	-0.141	0.052	3.172	3.446
3360	3360	17	Polyketide synthesis (I/III)	0.789	-0.342	0.276	-0.120	0.090	3.316	3.609
3361	3361	17	Polyketide synthesis (I/III)	0.743	-0.246	0.271	-0.113	0.006	3.223	3.495
3362	3362	17	Polyketide synthesis (I/III)	0.669	-0.347	0.271	-0.268	-0.058	3.200	3.411
aerA	223	17	Aeruginosin synthesis	-0.148	-0.025	0.079	0.269	0.094	-0.001	-0.233
224	224	17	Aeruginosin synthesis	0.066	0.083	0.327	0.376	0.104	0.436	0.361
225	225	17	Aeruginosin synthesis	0.002	0.053	0.296	0.340	0.095	0.445	0.321
aerB	226	17	Aeruginosin synthesis	0.007	0.084	0.180	0.376	0.217	0.292	0.156
228	228	15	Aeruginosin synthesis	-0.018	-0.048	0.259	0.347	0.232	0.449	0.328
aerD	229	17	Aeruginosin synthesis	0.035	-0.026	0.283	0.354	0.196	0.433	0.365
aerE	230	17	Aeruginosin synthesis	-0.098	-0.250	-0.073	0.197	0.066	0.220	0.034
aerF	231	17	Aeruginosin synthesis	-0.006	-0.165	0.047	0.313	0.153	0.353	0.217
232	232	17	Aeruginosin synthesis	-0.054	-0.046	0.180	0.440	0.294	0.253	0.074
aerG	233	17	Aeruginosin synthesis	0.010	-0.105	0.310	0.602	0.353	0.486	0.259
234	234	17	Aeruginosin synthesis	-0.021	-0.113	0.241	0.515	0.242	0.389	0.151
235	235	17	Aeruginosin synthesis	0.067	0.003	0.037	0.224	0.115	0.050	-0.017

Table S3.4 continued.

mcyJ	367	17	Microcystin synthesis	0.089	0.053	0.219	0.175	-0.014	-0.061	-0.025
mcyI	368	17	Microcystin synthesis	0.072	0.022	0.203	0.236	0.045	0.093	0.092
mcyH	369	17	Microcystin synthesis	-0.049	-0.117	-0.043	0.026	-0.008	-0.041	-0.177
mcyG	370	17	Microcystin synthesis	0.079	0.043	0.098	0.151	0.118	0.159	0.183
mcyF	371	17	Microcystin synthesis	0.108	-0.028	0.225	0.335	-0.026	0.084	0.028
mcyE	372	17	Microcystin synthesis	0.107	0.000	0.245	0.376	0.104	0.151	0.039
mcyD	373	17	Microcystin synthesis	-0.233	-0.113	-0.041	0.298	-0.035	-0.136	-0.421
mcyA	374	17	Microcystin synthesis	-0.131	-0.049	0.064	0.278	0.122	0.042	-0.157
mcyB	375	17	Microcystin synthesis	0.057	0.120	0.141	0.248	0.024	0.166	0.117
mcyC	377	17	Microcystin synthesis	0.091	0.128	0.309	0.418	0.163	0.236	0.163
mcaG	3995	17	Microcyclamide synthesis	-0.059	-0.152	-0.134	-0.137	-0.142	-0.071	-0.082
mcaF	3996	17	Microcyclamide synthesis	0.002	-0.026	0.040	0.059	0.229	0.275	0.250
mcaI	3998	17	Microcyclamide synthesis	-0.077	-0.152	-0.122	-0.110	-0.044	0.123	-0.017
mcaH	3999	17	Microcyclamide synthesis	-0.110	-0.199	-0.330	-0.278	-0.170	-0.027	-0.155
mcaE	4000	17	Microcyclamide synthesis	-0.042	0.259	0.059	-0.124	-0.415	-0.316	-0.215
mcaD	4004	17	Microcyclamide synthesis	-0.036	-0.120	-0.340	-0.254	-0.173	-0.259	-0.440
mcaC	4005	17	Microcyclamide synthesis	0.221	0.224	0.041	0.041	0.029	0.236	0.281
mcaB	4007	17	Microcyclamide synthesis	0.123	0.126	-0.010	-0.018	0.045	0.177	0.100
mcaA	4010	17	Microcyclamide synthesis	0.149	0.152	0.024	0.000	0.118	0.256	0.121
mcnC	3135	17	Cyanopeptolin synthesis	-0.030	-0.025	-0.001	0.033	0.000	-0.107	-0.213
mcnB	3136	17	Cyanopeptolin synthesis	-0.121	-0.109	-0.009	-0.076	-0.219	-0.145	-0.260
mcnA	3137	17	Cyanopeptolin synthesis	-0.167	-0.108	-0.068	-0.134	-0.343	-0.268	-0.379

Microcystis PCC 7806 was grown in chemostats at 200 ppm pCO_2 and subsequently exposed to 1450 ppm pCO_2.

[a]The IPF numbers are the locus tags of *Microcystis* PCC 7806 in the EMBL database (AM778843-AM778958).

[b]The function categories are based on CyanoBase, which has grouped genes into 18 categories (http://genome.microbedb.jp/cyanobase/Synechocystis/genes/category): (1) amino acid biosynthesis; (2) biosynthesis of cofactors, prosthetic groups, and carriers; (3) cell envelope; (4) cellular processes; (5) central intermediary metabolism; (6) energy metabolism; (7) fatty acid, phospholipid and sterol metabolism; (8) photosynthesis, and respiration; (9) purines, pyrimidines, nucleosides, and nucleotides; (10) regulatory functions; (11) DNA replication, restriction, modification, recombination, and repair; (12) transcription; (13) translation; (14) transport and binding proteins; (15) other categories; (16) hypothetical; (17) unknown.

[c]Log2 values quantify gene expression at the given time point (in h after increasing the pCO_2) with respect to gene expression at $t = 0$ (just before increasing the pCO_2). The presented log2 values are the average values of multiple probes per gene and four biological replicates (chemostats).

Grey shading indicates significant changes in gene expression ($p < 0.01$), where p-values were adjusted for multiple hypothesis testing. The complete table (including the p-values) is provided in the Supplementary Material of Sandrini *et al.* (2015a). *Frontiers in Microbiology* **6:** 401. doi: 10.3389/fmicb.2015.00401.